Ocean Modelling xxx (2012) xxx–xxx

Contents lists available at SciVerse ScienceDirect

Ocean Modelling

journal homepage: www.elsevier.com/locate/ocemod

Validation of a thirty year wave hindcast using the Climate Forecast System Reanalysis winds ☆

Arun Chawla [a,*], Deanna M. Spindler [b], Hendrik L. Tolman [a]

[a] NOAA/NCEP, Environmental Modeling Center, College Park, MD 20740, United States
[b] IMSG at NOAA/NCEP, Environmental Modeling Center, College Park, MD 20740, United States

ARTICLE INFO

Article history:
Available online xxxx

Keywords:
Waves
Hindcasts
Reanalysis
WAVEWATCH III
Wind wave models
Validation

ABSTRACT

A thirty one year wave hindcast (1979–2009) using NCEP's latest high resolution Climate Forecast System Reanalysis (CFSR) wind and ice database has been developed and is presented here. The hindcast has been generated using the third generation wind wave model WAVEWATCH III® with a mosaic of 16 two-way nested grids. The resolution of the grids ranged from 1/2° to 1/15°. Validation results for bulk significant wave height H_s and 10 m (above Mean Sea Level) wind speeds U_{10} have been presented using both altimeter records and NDBC buoys. In general the database does a good job of representing the wave climate. At most buoys there is excellent agreement between model and data out to the 99.9th percentile. The agreement at coastal buoys is not as good as the offshore buoys due to unresolved coastal features (topographic/bathymetric) as well as issues related to interpolating wind fields at the land-sea margins. There are some concerns about the wave climate in the Southern Hemisphere due to the over prediction of winds (early part of the database) as well as the lack of wave blocking due to icebergs (in the model).

Published by Elsevier Ltd.

1. Introduction

Long-term global wind wave databases have multiple scientific and engineering applications, such as developing wave climatologies, long-term statistical analysis for engineering design, scenario studies, and validation of model physics. The wave modeling group at the National Center for Environmental Prediction (NCEP) maintains a wave hindcast database that extends from 1999 to the present. This database uses the archived analysis winds from the GFS atmospheric model (Moorthi et al., 2001) to drive the waves. However, this database is statistically inhomogeneous because numerical and physical upgrades to the models (both wave and atmosphere) are responsible for trends, and therefore the database should not be used for climate studies. In atmospheric modeling, a statistically more homogeneous dataset can be generated by performing a reanalysis with a consistent model setup for the entire period covered (e.g. Saha et al., 2010).

There are not enough available data to develop a traditional reanalysis for wind waves. Furthermore, wave dynamics are different from atmospheric dynamics in the sense that they represent a forced and damped problem rather than a (chaotic) initial value problem, with the wind forcing being the dominant process driving wave dynamics. Due to the forced and damped nature of wind waves, it is possible to produce accurate hindcast without assimilating any wave data, for instance using a wind field from a long-term reanalysis project. There are several such examples in literature. Sterl et al. (1998) used a 15 year reanalysis wind field from the European Center for Medium-Range Weather Forecasting (ECMWF) to build a hindcast wave database. This was further expanded into a coupled 40 year reanalysis that included assimilation of both atmospheric and wave data (Uppala et al., 2005). Using a separate reanalysis wind field from NCEP/NCAR, Cox and Swail (2001) developed a global 40 year wave hindcast. However, due to resource limitations, historically reanalysis winds have been developed on temporal and spatial grids that are too coarse to resolve some of the major events that drive the stronger waves. Some attempts have been made to correct for this using a kinematic reanalysis of the winds and subsequent hindcast (Swail and Cox, 2000), as well as non-parametric corrections to the wave field using training sets (Caires and Sterl, 2005). A detailed inter comparison of early reanalysis data sets is provided in Caires et al. (2004).

A new NCEP Climate Forecast System Reanalysis (CFSR) has recently been developed and entails a coupled reanalysis of the atmospheric, oceanic (only circulation), sea-ice and land data from 1979 to 2010 (Saha et al., 2010). This reanalysis has much higher spatial and temporal resolutions than previous reanalyses, and thus provides a valuable resource to develop a long-term hindcast database for wind waves. NCEP has chosen to perform wave hindcasts without data assimilation to avoid inhomogeneities in quality of the product associated with severe sparsity of observation data. We believe that a more homogeneous 'assimilative' product can be

☆ MMAB Contribution No. 299.

* Corresponding author.
E-mail address: arun.chawla@noaa.gov (A. Chawla).

1463-5003/$ - see front matter Published by Elsevier Ltd.
http://dx.doi.org/10.1016/j.ocemod.2012.07.005

generated by using observations to produce bias corrections for a hindcast, but the latter is considered outside the scope of this study.

The wave model used at NCEP is the third generation wind wave model WAVEWATCH III® (Tolman, 2009). In 2007, the model was expanded to run as a mosaic of two-way nested grids (Tolman, 2008). The nested grid driver is described in Tolman (2007a,b). To drive the waves the wave model requires two input fields: ice and winds (including the air–sea temperature difference). The high resolution global winds at 10 m height used here have an hourly temporal and 1/2° spatial resolution. The reanalysis daily ice concentration fields have a 1/2° spatial resolution, and are derived from passive microwave from the SMMR and SSM/I using the NASA Team algorithm.

The hindcast database has been developed taking advantage of the multi-grid features in WAVEWATCH III with finer resolution grids in coastal waters and semi-enclosed basins like the Mediterranean Sea, to provide adequate resolution for wave evolution, or to spatially resolve areas with in situ observations. This paper describes the wave database as well as model validation using both altimeters and buoy data. The error metrics used to quantify model skill are given in Appendix A.

2. Validation datasets

Validation studies in this paper have been done using two sources of data; the quality controlled altimeter data archive maintained at IFREMER (Queffeulou, 2004) and the historical buoy data archive from the National Data Buoy Center (NDBC). Fig. 1 shows the temporal extent of all the altimeter records used in the analysis. To facilitate comparison with altimeter tracks, hourly gridded model results (significant wave height H_s and wind speeds 10 m above Mean Sea Level U_{10}) are interpolated in space and time on to the altimeter tracks. A 15 point running average (equivalent to the resolution of the 1/2° global grid defined in Section 3) is used to filter the altimeter data. Statistical estimates were made using three months of track data to provide large enough sample sizes for statistically significant results. Spatially the track data were either binned into $2^\circ \times 2^\circ$ boxes (for error maps) or grouped by region (for regional error metrics).

Since no altimeter data are available for the earlier periods of the hindcast runs (prior to 1991), validation was also done using select buoy records from NDBC (Fig. 2). These buoys were selected because they are representative of the region and for the length of their records. Validation statistics are primarily limited to U_{10} and H_s. To reduce sampling errors associated with finite length records (Foristall et al., 1996), the hourly buoy H_s data have been filtered using a 3 point running average. In those buoy records where wind data are available, wind speeds are converted from the anemometer height to U_{10} assuming a neutrally stable boundary layer at the ocean–air interface. The same smoothing that is applied to the H_s data is also applied to the U_{10} data as well. While the validation studies in this paper are limited to a select set of buoys, a separate report with validation plots from more than 130 buoys has been provided as support material for this manuscript. This material is available online together with the electronic version of the manuscript in the Elsevier web products.

3. Model setup

3.1. Grids

The WAVEWATCH III model can be run as a mosaic of overlapping grids with two-way interaction between the higher and lower

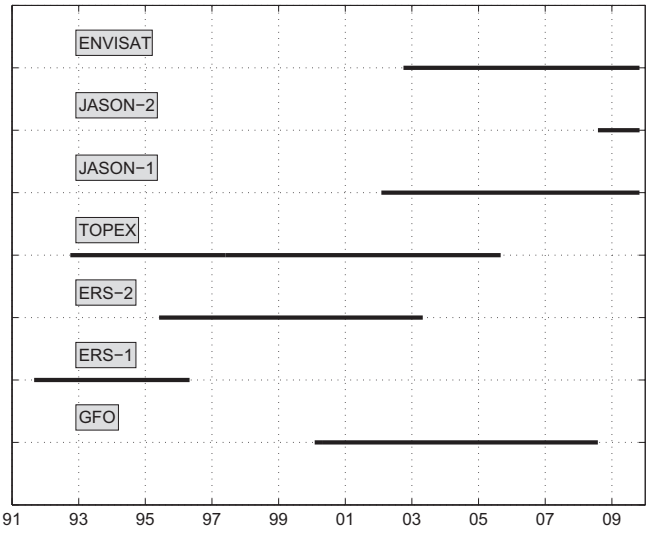

Fig. 1. Available altimeter records from the different instruments. *x*-axis represents years in YY format.

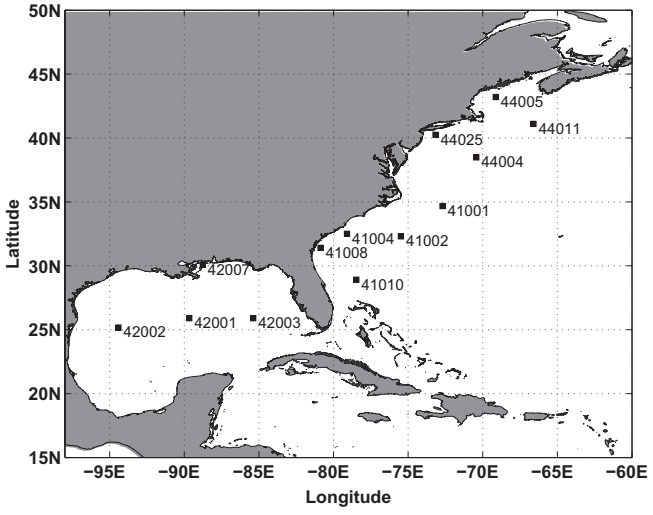

(a) Atlantic/Gulf of Mexico Buoys

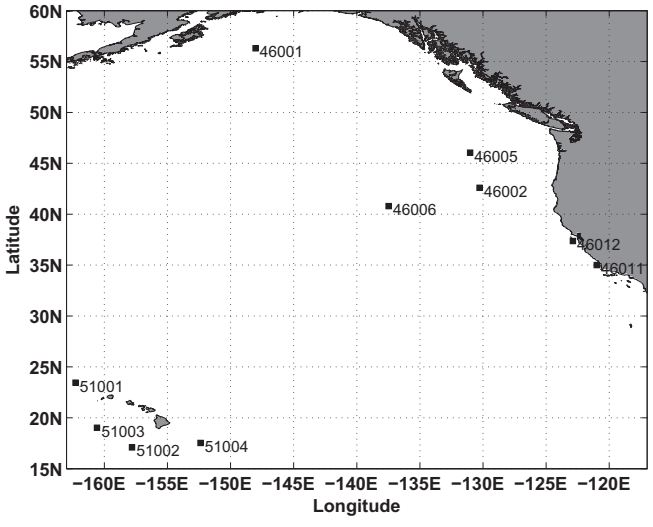

(b) Pacific/Hawaii Buoys

Fig. 2. Location of NDBC buoys used in the validation.

Please cite this article in press as: Chawla, A., et al. Validation of a thirty year wave hindcast using the Climate Forecast System Reanalysis winds. Ocean Modell. (2012), http://dx.doi.org/10.1016/j.ocemod.2012.07.005

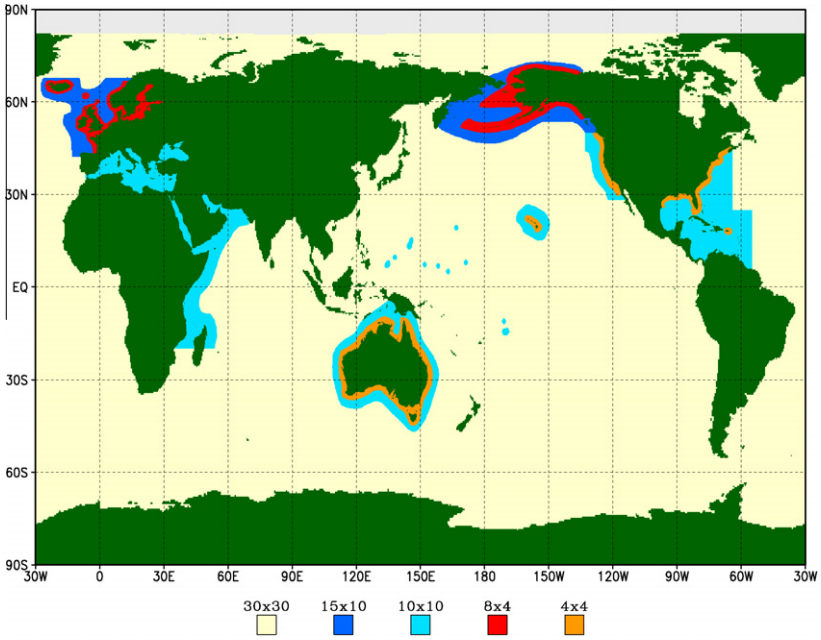

Fig. 3. Global domain. Grid resolution in arc-minutes.

Table 1
WAVEWATCH III grid particulars. All output data associated with a particular grid are identified by their grid labels.

Name	Grid label	Latitude	Longitude	Resolution (lat × lon)
Global	glo_30m	90°S:90°N	180°E:180°W	1/2° × 1/2°
Arctic	ao_30m	55°N:90°N	180°E:180°W	1/2° × 1/2°
Mid-Globe	mid_30m	65°S:65°N	180°E:180°W	1/2° × 1/2°
Antarctic	ac_30m	90°S:55°S	180°E:180°W	1/2° × 1/2°
East Coast US	ecg_10m	0°N:55°N	100°W:50°W	1/6° × 1/6°
West Coast US	wc_10m	25°N:50°N	150°W:110°W	1/6° × 1/6°
Alaska	ak_10m	44°N:75°N	140°E:120°W	1/6° × 1/4°
Pacific Isl	pi_10m	20°S:30°N	130°E:145°W	1/6° × 1/6°
Australia	oz_10m	50°S:0°N	105°E:165°E	1/6° × 1/6°
North Sea	nsb_10m	42°N:75°N	28°W:31°E	1/6° × 1/4°
Mediterranean	med_10m	30°S:48°N	7°W:43°E	1/6° × 1/6°
NW Indian O	nwio_10m	20°S:31°N	30°E:70°E	1/6° × 1/6°
East Coast US	ecg_4m	15°N:47°N	101°W:60°W	1/15° × 1/15°
West Coast US	wc_4m	15°N:50°N	165°W:116°W	1/15° × 1/15°
Alaska	ak_4m	48°N:74°N	165°E:122°W	1/15° × 2/15°
Australia	oz_4m	50°S:0°N	105°E:165°E	1/15° × 1/15°
North Sea	nsb_4m	42°N:68°N	28°W:31°E	1/15° × 2/15°

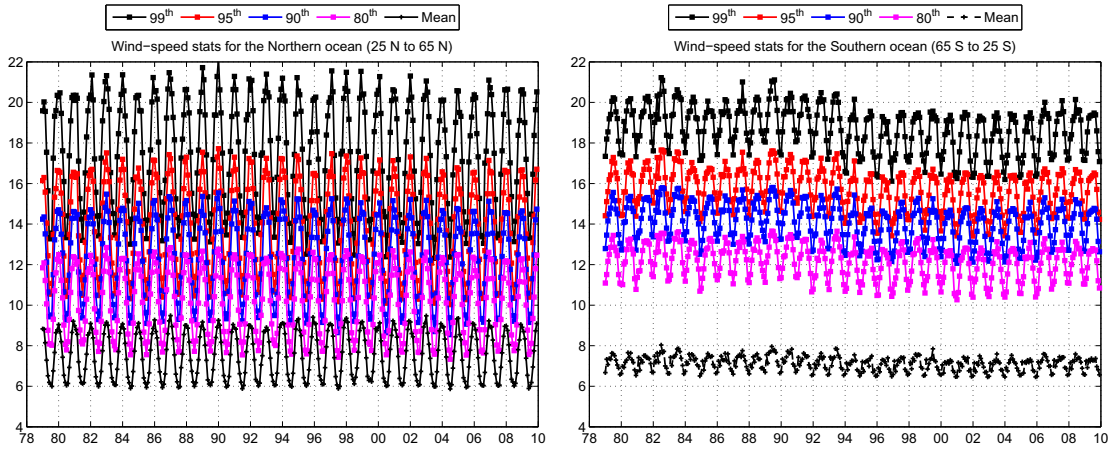

Fig. 4. Monthly U_{10} wind speeds (in m/s) at percentiles of occurrence from the CFSR database for the Northern (left panel) and Southern (right panel) hemispheres. *x*-axis represents years in YY format.

Please cite this article in press as: Chawla, A., et al. Validation of a thirty year wave hindcast using the Climate Forecast System Reanalysis winds. Ocean Modell. (2012), http://dx.doi.org/10.1016/j.ocemod.2012.07.005

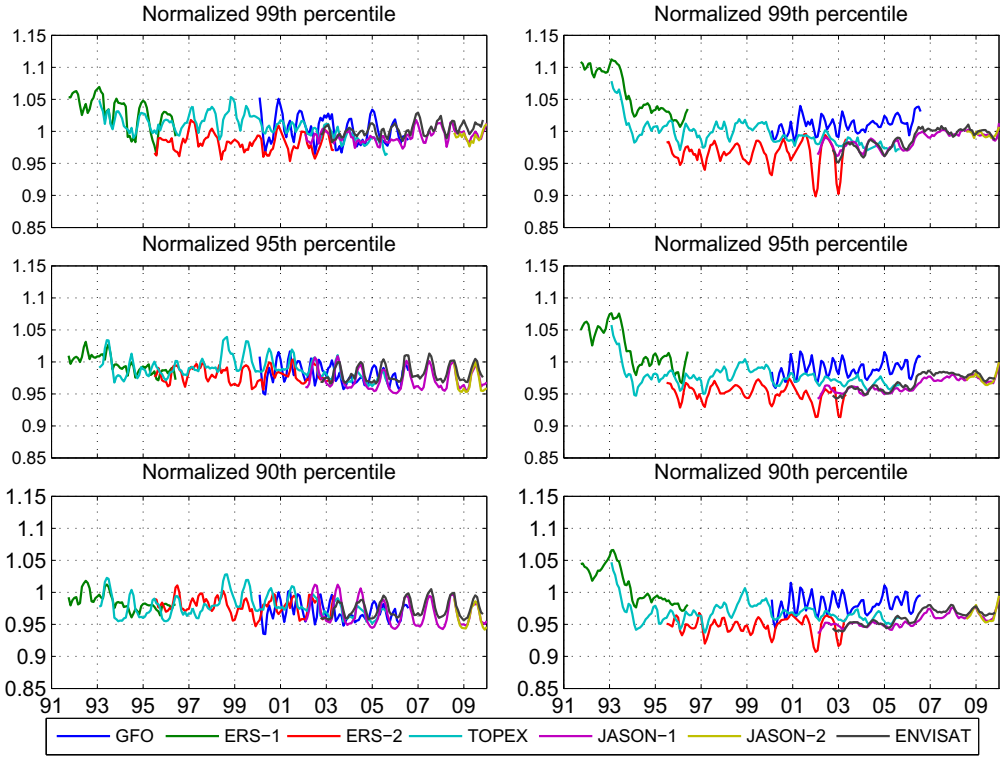

Fig. 5. Normalized U_{10} at percentiles for the Northern (left panels) and Southern (right panels) Hemispheres. Wind speeds from the model (CFSR database) have been normalized with the wind speeds at corresponding percentiles from the altimeters. Percentiles have been computed along the altimeter tracks. See Section 2 for details on how statistics are computed from the altimeters.

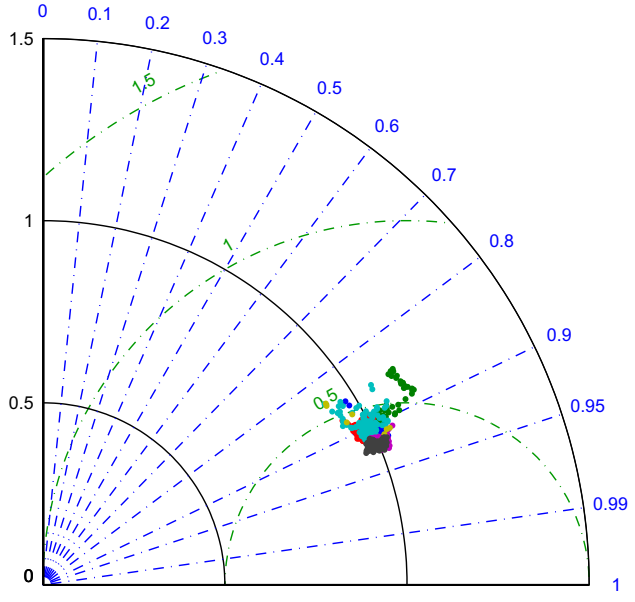

Fig. 6. A Taylor diagram of error metrics for U_{10} for all the different altimeters. Color scheme for the altimeters is the same as in Fig. 5. The radial blue lines represent correlation coefficients (ρ), the solid black circular contours represent the normalized standard deviation (σ_n) and the dashed contour lines represent the normalized centered RMS error (*CRMSE*). See Appendix A for the definitions of these metrics. Each dot represents estimates made over all the tracks in a 3 month window. A perfect model data comparison would lie along *x*-axis on the 1 solid line contour. (For interpretation of the references to color in this figure legend, the reader is referred to the web version of this article.)

resolution grids. This facilitates increased computational efficiencies by restricting the higher resolution grids only in areas of interest.

Table 2
Error statistics for H_s and U_{10} at select NDBC buoy locations (see Fig. 2 for buoy locations). Statistics have been computed over the entire hindcast period (wherever data is available). Except for *SI* and R^2 estimates (which are non-dimensional) all other error metrics are in m for H_s and m/s for U_{10}.

Buoy	Bias (H_s, U_{10})	SI	RMSE	R^2
Atlantic/Gulf of Mexico buoys				
41008	(−0.02, −0.28)	(21.7, 29.2)	(0.21, 1.77)	(0.81, 0.66)
41004	(0.02, 0.03)	(21.9, 23.5)	(0.29, 1.65)	(0.83, 0.78)
41010	(0.08, −0.16)	(19.0, 20.6)	(0.31, 1.36)	(0.87, 0.82)
41002	(0.08, 0.18)	(19.7, 21.5)	(0.37, 1.54)	(0.87, 0.82)
41001	(0.06, 0.09)	(19.3, 21.3)	(0.40, 1.65)	(0.88, 0.82)
44004	(0.08, 0.33)	(19.8, 22.0)	(0.41, 1.76)	(0.90, 0.82)
44025	(−0.04, 0.20)	(23.5, 22.6)	(0.30, 1.59)	(0.83, 0.81)
44005	(−0.25, 0.53)	(31.0, 26.8)	(0.55, 2.00)	(0.76, 0.77)
44011	(−0.01, 0.90)	(18.5, 24.3)	(0.37, 1.86)	(0.91, 0.82)
42001	(0.15, −0.40)	(23.2, 22.0)	(0.30, 1.47)	(0.89, 0.80)
42002	(0.12, 0.08)	(24.4, 24.3)	(0.33, 1.55)	(0.84, 0.73)
42003	(0.02, −0.41)	(24.4, 22.5)	(0.26, 1.48)	(0.88, 0.80)
42007	(−0.09, −0.97)	(32.3, 28.9)	(0.22, 1.97)	(0.80, 0.65)
Pacific/Hawaii buoys				
46001	(0.10, 0.19)	(17.5, 9.2)	(0.49, 1.55)	(0.89, 0.85)
46005	(0.36, 0.06)	(16.2, 18.7)	(0.57, 1.46)	(0.92, 0.85)
46002	(0.33, 0.11)	(15.5, 17.5)	(0.54, 1.33)	(0.92, 0.85)
46006	(0.37, −0.26)	(15.4, 17.4)	(0.57, 1.44)	(0.93, 0.87)
46012	(0.43, −0.12)	(18.8, 32.0)	(0.58, 1.83)	(0.84, 0.68)
46011	(0.28, −1.26)	(18.7, 34.8)	(0.48, 2.42)	(0.82, 0.63)
51001	(0.24, −0.19)	(16.9, 16.0)	(0.48, 1.17)	(0.85, 0.82)
51003	(0.13, −0.43)	(17.5, 19.2)	(0.41, 1.32)	(0.76, 0.69)
51002	(0.22, −0.34)	(15.9, 14.2)	(0.44, 1.23)	(0.76, 0.78)
51004	(0.15, −0.41)	(12.0, 14.2)	(0.33, 1.20)	(0.82, 0.75)

Overall, the global domain was separated into sixteen computational grids (Fig. 3). These grids were developed using ETOPO1 bathymetry (Amante and Eakins, 2009) together with v 1.10 of the Global Self-consistent Hierarchical High resolution Shoreline (GSHHS) database. See Chawla and Tolman (2007, 2008) for details on the software used for developing these grids. Individual grid

details are provided in Table 1. Grids of three different resolutions were generated: coarse resolution (1/2° or 30 arc-min), intermediate resolution (1/6° or 10 arc-min), and fine resolution (1/15° or 4 arc-min). The 1/2° grids wrap around the globe (in longitude). All the grids are regular spherical grids and as a result, model time steps are limited by the CFL criteria. For increased efficiency, the global domain is represented by three overlapping grids – an Arctic grid (ao_30m; as defined in Table 1), an Antarctic grid (ac_30m) and a grid for the middle part of the domain (mid_30m). This was done to confine the smaller time steps needed near the poles to a set of smaller grids. For convenience the output from these three grids is gathered in a single global grid (glo_30m). To avoid the singularity at the poles, all grid points beyond 82°N in ao_30m are marked as inactive.

The spectral domain has been divided into 50 frequency and 36 directional bins (directional resolution of 10°). The minimum frequency has been set at 0.035 Hz and the frequency increment factor has been set at 1.07, providing a frequency range of 0.035–0.963. A parametric tail is fitted beyond the highest computed frequency. At specified output points (corresponding to buoy locations and other points of interest) spectral data are linearly interpolated from the surrounding grid points on an hourly time scale. For points that are located in multiple grids, the data are extracted from the highest resolution grid.

3.2. Physics packages

The physics packages used in the development of this database have been used in operational forecasting and hindcasting at NCEP for the better part of the last decade. These packages are listed below and more details can be found in Tolman (2009).

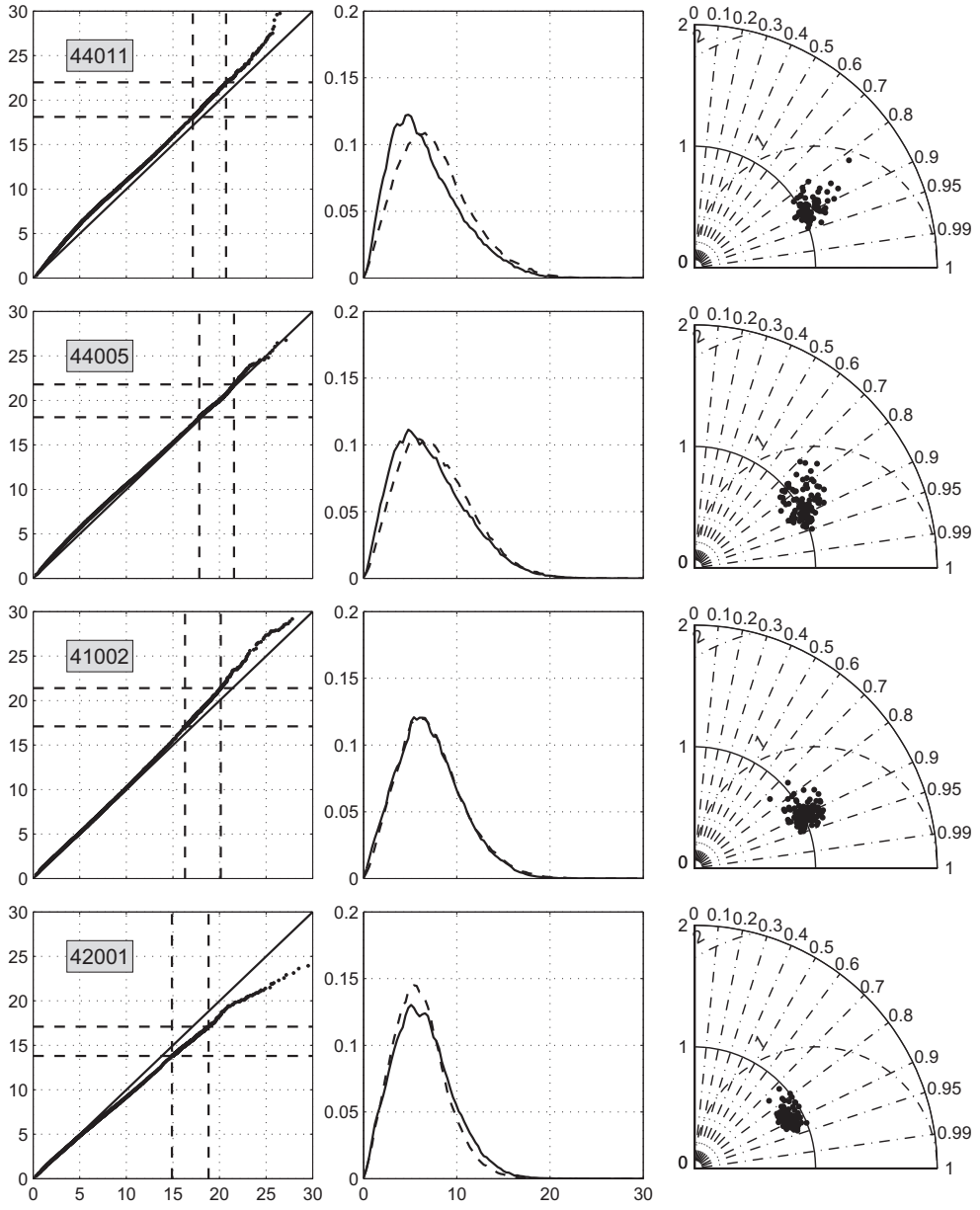

Fig. 7. U_{10} (in m/s) distribution at select buoys in the Atlantic Ocean. The first column of panels represent Q–Q plots with model velocities along the *y*-axis and data along the *x*-axis. The vertical (horizontal) dashed lines represent the 99th and 99.9th percentiles for data (model). The middle column of panels represents the PDF of U_{10}, with solid lines representing data and dashed lines representing model. The third column of panels represent Taylor diagram representations of monthly statistics.

Please cite this article in press as: Chawla, A., et al. Validation of a thirty year wave hindcast using the Climate Forecast System Reanalysis winds. Ocean Modell. (2012), http://dx.doi.org/10.1016/j.ocemod.2012.07.005

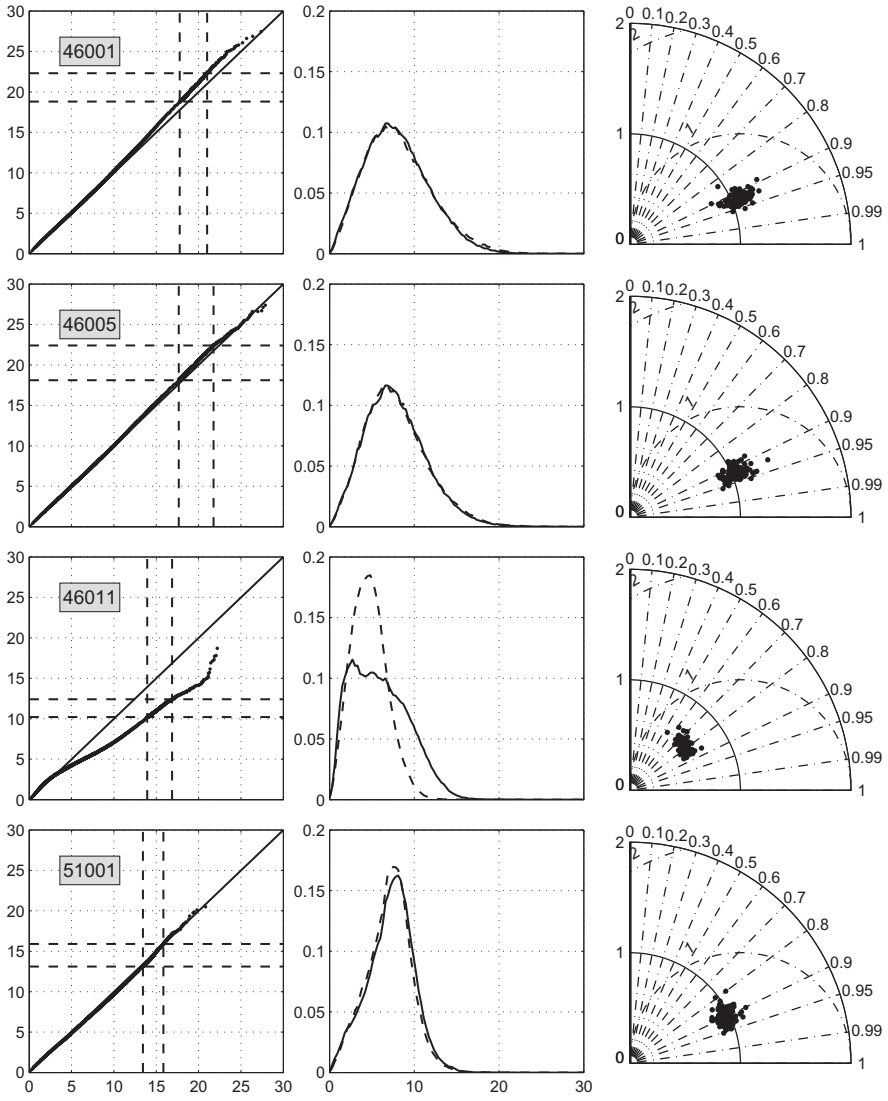

Fig. 8. Like Fig. 7 but for buoys in the Pacific Ocean. U_{10} units are in m/s.

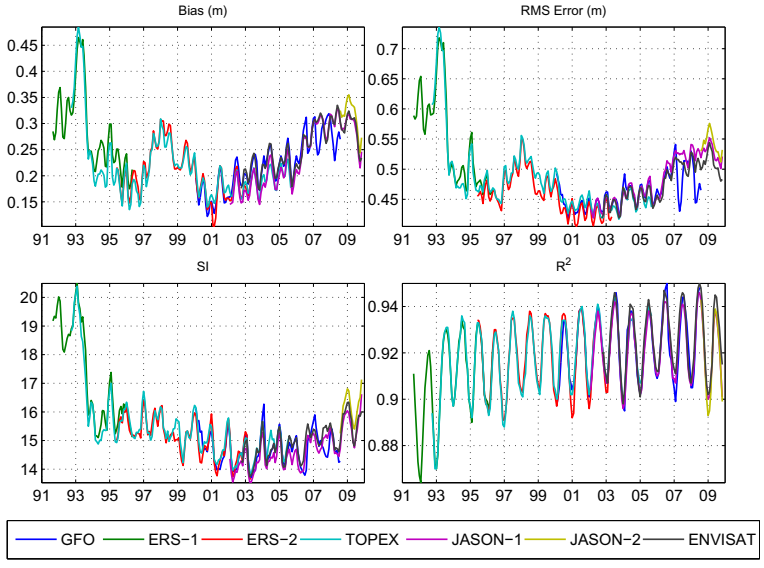

Fig. 9. H_s error metrics (in m for the dimensional metrics) from the different altimeters. Monthly statistics are computed over a sliding 3 month period for the global domain. Metric definitions are given in Appendix A.

Please cite this article in press as: Chawla, A., et al. Validation of a thirty year wave hindcast using the Climate Forecast System Reanalysis winds. Ocean Modell. (2012), http://dx.doi.org/10.1016/j.ocemod.2012.07.005

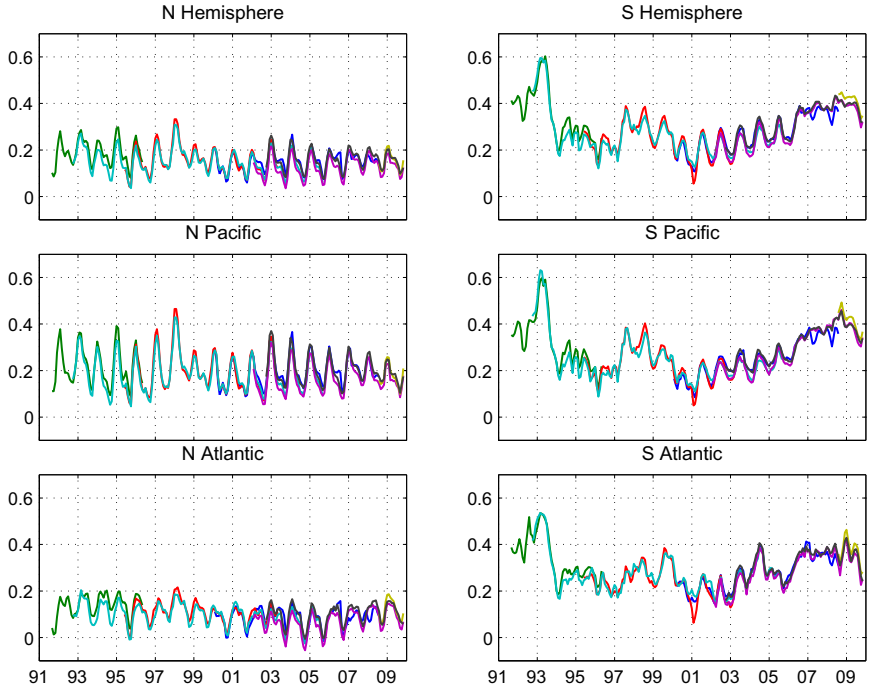

Fig. 10. H_s biases (in m) from the different altimeters for different regions of the globe. Statistics are computed as in Fig. 9. Color scheme is the same as in Fig. 9.

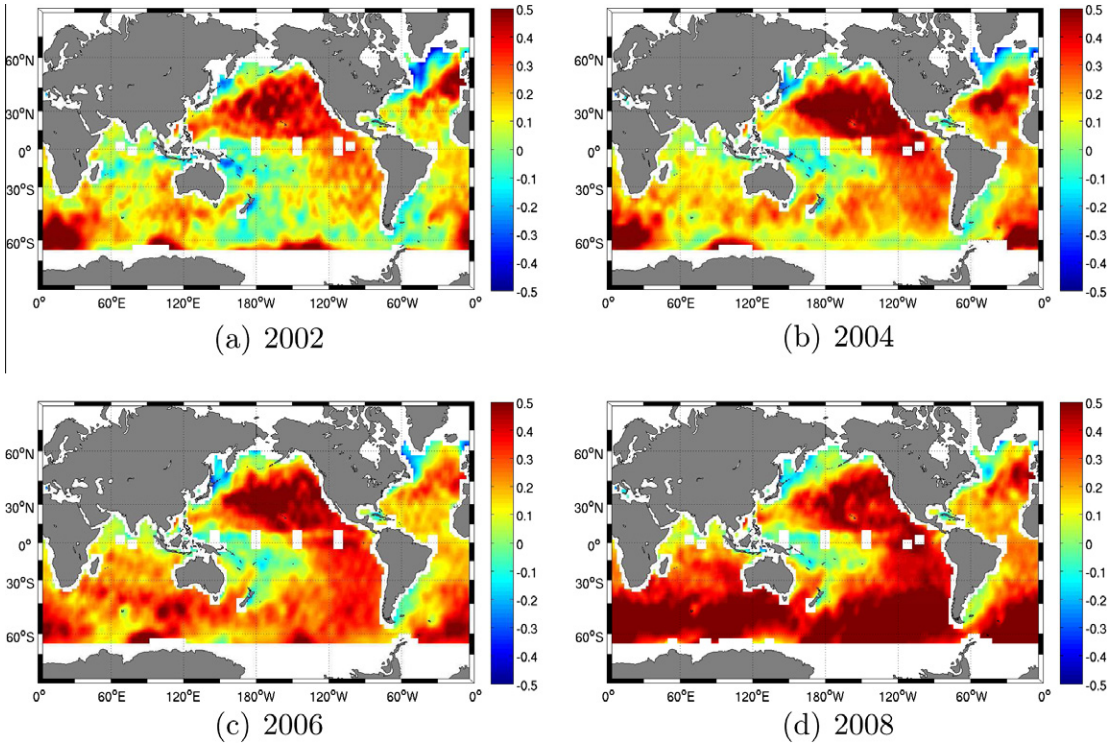

Fig. 11. H_s bias maps (in m) from the Jason 1 satellite tracks for select years during the months of December–February. The maps have been made using three months of collocated model-data values along the altimeter tracks and binning them in $2^\circ \times 2^\circ$ bins.

- The Tolman-Chalikov source term package (Tolman and Chalikov, 1996) with stability correction and a cap for maximum drag.
- DIA approximation (Hasselmann et al., 1985) for non-linear interactions. (Note that while the original DIA was built assuming a spectral increment factor of 1.1, changing that to 1.07 had no discernible impact on spectral evolution.)
- Battjes-Janssen shallow water depth breaking (Battjes et al., 1978) with a Miche-style shallow water limiter for maximum energy.
- ULTIMATE QUICKEST (Leonard, 1979, 1991; Davis and More, 1982) propagation scheme with averaging technique for Garden Sprinkler alleviation (Tolman, 2002a).

Please cite this article in press as: Chawla, A., et al. Validation of a thirty year wave hindcast using the Climate Forecast System Reanalysis winds. Ocean Modell. (2012), http://dx.doi.org/10.1016/j.ocemod.2012.07.005

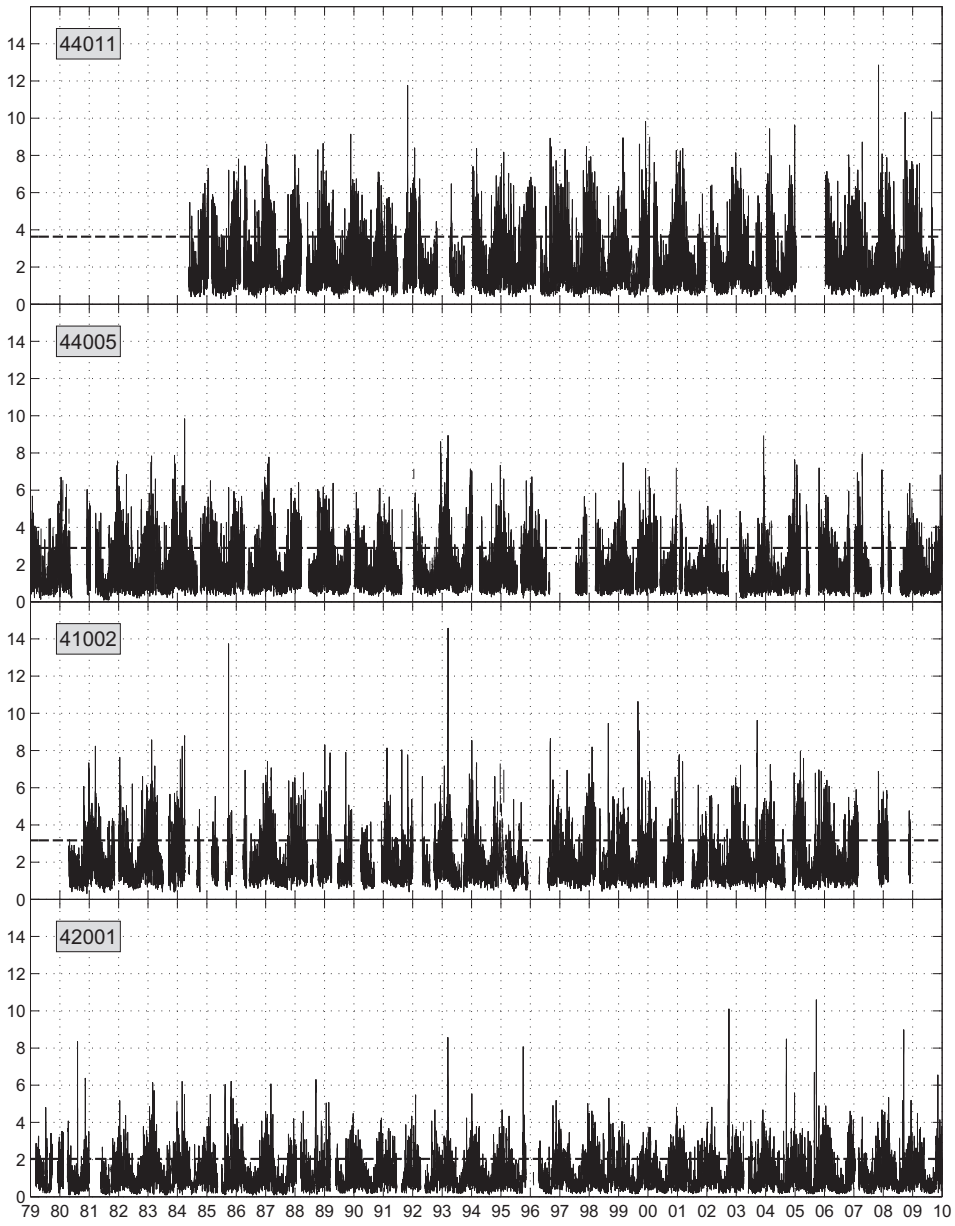

Fig. 12. H_s time series (in m) at select buoys in the Gulf of Mexico and Atlantic Ocean. See Fig. 2 for buoy locations. Dashed lines represent H_s values at the 90th percentile (computed from data) that are used as cut-off for peak event analysis (Figs. 18 and 19).

- JONSWAP bottom friction formulation (Hasselmann et al., 1973) with no bottom scattering.

4. CFSR winds

The new NCEP Climate Forecast System Reanalysis (CFSR) entails a coupled reanalysis of the atmospheric, oceanic, sea-ice and land data from 1979 to 2010, and a reforecast run with this reanalysis after that (Saha et al., 2010). Here, only the reanalysis results will be used. The CFSR represents a significant upgrade from the older reanalyses done at NCEP (Kalnay et al., 1996; Kanamitsu et al., 2002). It has a much finer horizontal resolution (≈38 km as opposed to the earlier ≈200 km) and more vertical layers for the atmosphere (64 as opposed to 28). It is also coupled to an ocean circulation model (as opposed to using a prescribed Sea Surface Temperature (SST) over the ocean as was done earlier).

A detailed evaluation of reanalysis winds is beyond the scope of this paper (readers are referred to the original article). However, since the 10 m (above MSL) winds are the main driving force for ocean waves, some analysis of these winds is performed here. Cox et al. (2011) also addressed the feasibility of the CFSR winds for oceanographic forcing. Both buoy and altimeter data are used here for validating U_{10}. Even though altimeter data provide an indirect measure of the wind speed (Caires and Sterl, 2003), they are valuable independent data sets to compare against the winds (altimeter winds are not assimilated into the CFSR).

Fig. 4 shows the monthly wind speeds at percentiles of occurrence for the Northern and Southern Hemispheres from the CFSR. The Northern Hemisphere shows consistent wind fields for the length of the database. Some of the inter-annual oscillations at the higher wind speeds may be related to El-Nino/La-Nina cycles and associated storm activities. The Southern Hemisphere on the other hand shows a clear transition around 1993–1994, where

Please cite this article in press as: Chawla, A., et al. Validation of a thirty year wave hindcast using the Climate Forecast System Reanalysis winds. Ocean Modell. (2012), http://dx.doi.org/10.1016/j.ocemod.2012.07.005

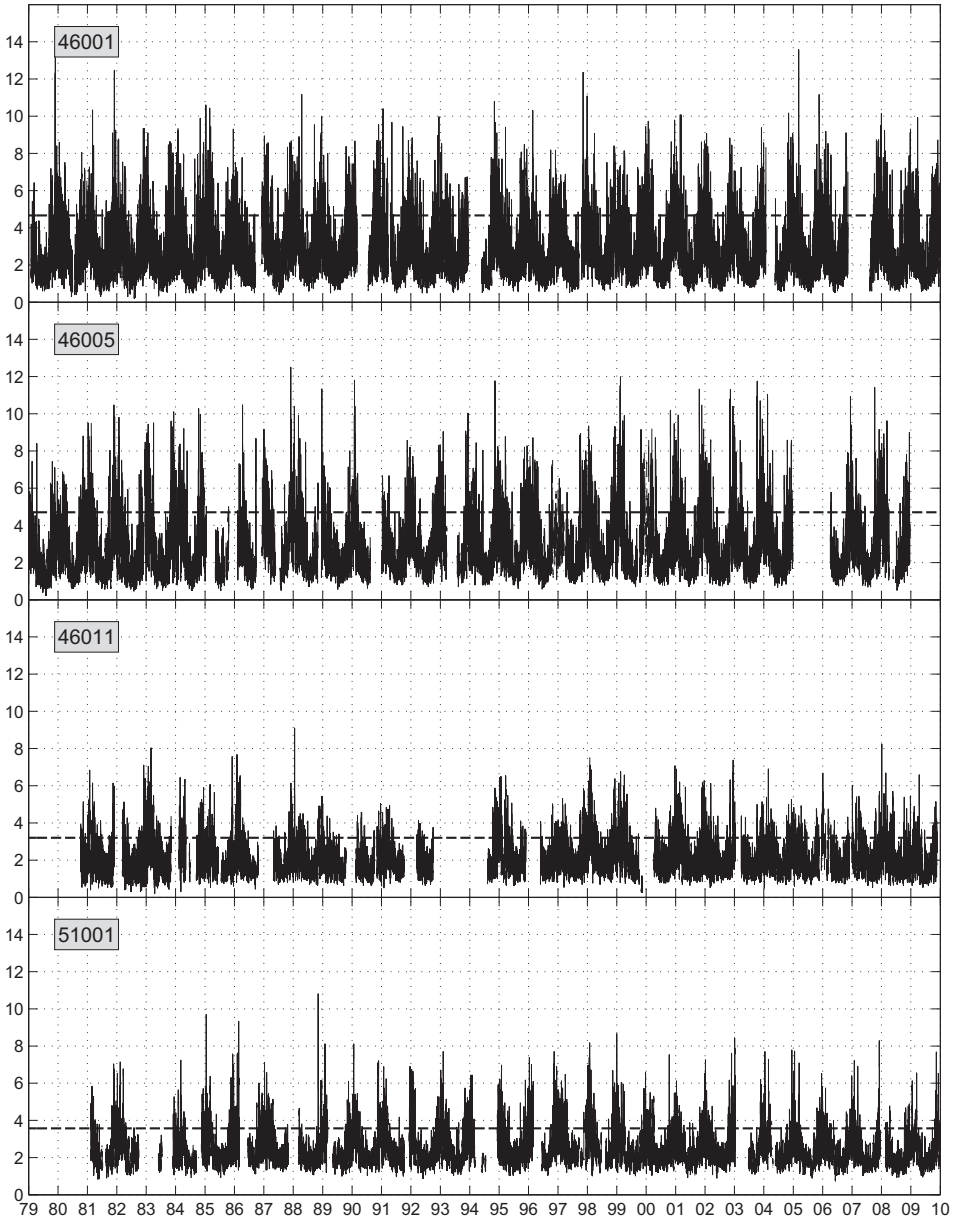

Fig. 13. Like Fig. 12 but for buoys in the Pacific Ocean. H_s units in m.

the higher percentile winds prior to that are stronger than the winds after that. This transition coincides with the introduction of Special Sensor Microwave Imager (SSM/I) derived ocean surface wind observations in CFSR (Saha et al., 2010). There is a second smaller jump in winds speed for higher percentiles of occurrence in 2006. This transition does not seem to coincide with the introduction of any ocean surface wind data though a number of satellite radiance data streams were added to the CFSR analysis in 2006 see Fig. 4 in Saha et al. (2010). These transitions in wind speeds are the strongest in the 99th percentile winds. Apart from these transitions, Fig. 4 shows that the seasonal variability (in wind speeds) is much greater in the Northern Hemisphere than the Southern Hemisphere with the seasonal maxima being fairly similar in both hemispheres but the seasonal minima in the Northern Hemisphere being much lower. These are driven by the different land masses in the two regions, creating stronger winter (as indicated by the higher 99th percentile winds) and weaker summer conditions in the Northern Hemisphere. Stopa et al. (submitted for publication) provide a detailed seasonal analysis of the CFSR wind patterns in the two hemispheres.

Comparing the percentiles with the limited available altimeter data (Fig. 5) shows that prior to 1993–1994, the stronger winds are clearly overestimated in the Southern Hemisphere. The scatter in the plots is a reflection of the different algorithms used to estimate wind speeds in the different platforms. However, the trends are clearly visible across all the platforms. Also note that while in Fig. 4 the percentiles are computed from wind speeds over the entire regional domain, in Fig. 5 the percentiles are computed along altimeter tracks only. One concern is that the comparisons have been done using altimeter data that are accurate in wind speeds of 1–20 m/s (Gourrion et al., 2002), and the 99th percentile winds in the Southern Hemisphere are at the upper limits of this range (Fig. 4). But since this over estimation is observed in winds down to the 90th percentile, it is a valid feature of the CFSR winds in

Please cite this article in press as: Chawla, A., et al. Validation of a thirty year wave hindcast using the Climate Forecast System Reanalysis winds. Ocean Modell. (2012), http://dx.doi.org/10.1016/j.ocemod.2012.07.005

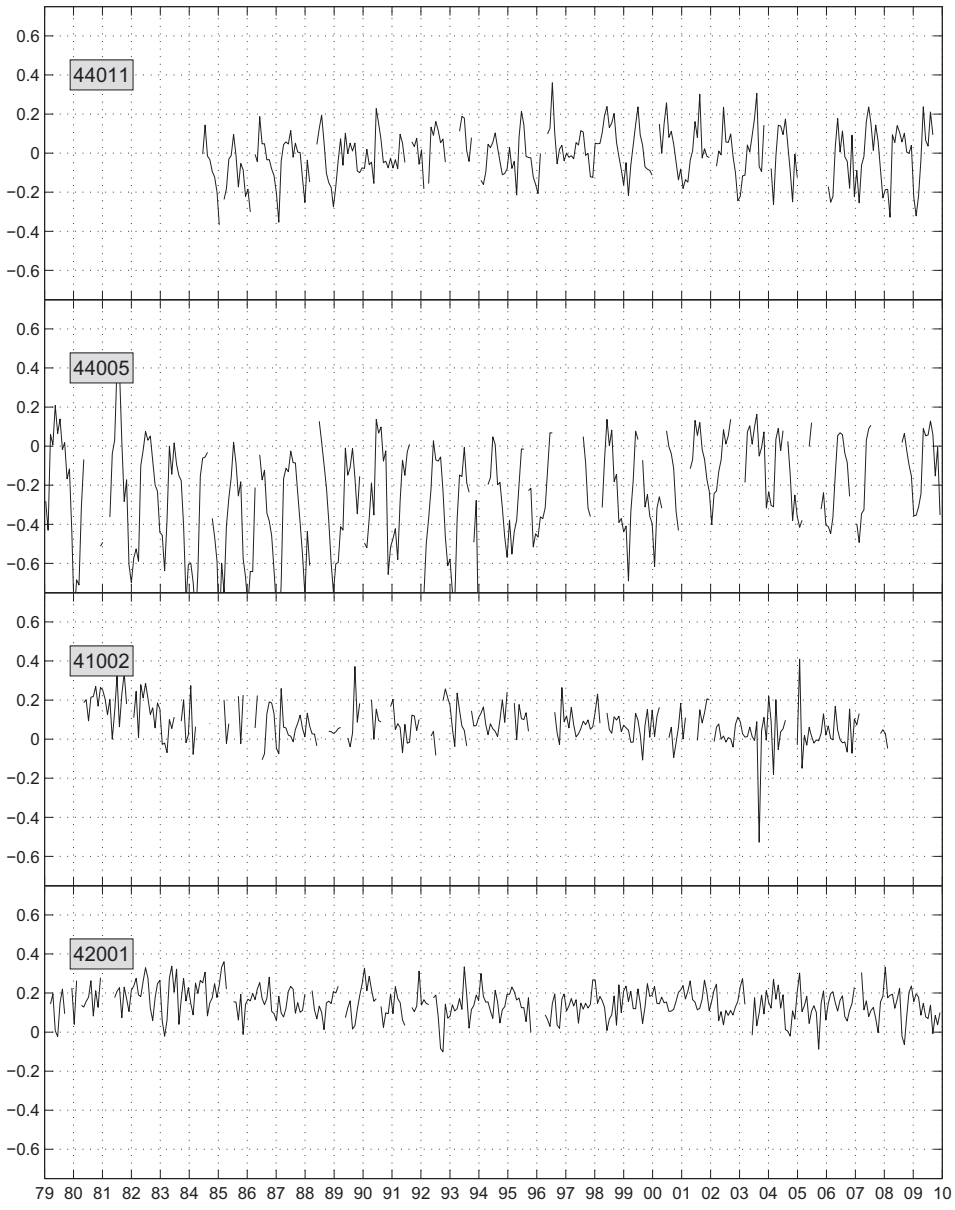

Fig. 14. Monthly mean H_s biases (in m) at the buoys corresponding to Fig. 12. Biases are computed from the hourly model-data pairs. Bias for any particular month segment is only computed if there are more than 350 such pairs (≈14 days) in the segment.

the Southern Hemisphere. As shall be shown below, this has a significant impact on the underlying waves since the stronger winds are the predominant drivers of wave growth.

A Taylor diagram (Taylor, 2001) provides a convenient way to represent multiple statistical metrics of model-data comparisons on the same plot, but has generally not been used in wave modeling. Fig. 6 provides such a representation of the collocated CFSR and altimeter wind speeds for all the available altimeter sets. Most of the time the correlation is on the order of 0.9 or better. And with the exception of the data prior to 1994 the normalized standard deviation is clustered around 1, indicating that the energetic components of the winds are well represented in the data.

For completeness, comparisons have also been done with the NDBC buoys and Table 2 lists the statistics over the entirety of the record for each station used in the analysis. Figs. 7 and 8 show the U_{10} distributions for a select number of buoys in the Atlantic and Pacific Oceans. In general, the winds are well represented with correlation coefficients of 0.8 or higher. The exceptions are buoys close to the coast (see buoy 46011 in Fig. 8 and Table 2). Some of this is a reflection of the way winds are being interpolated. In the current database it is a simple linear interpolation that does not account for land-sea transitions. This can be a problem in coastal areas dominated by local wind seas. The other region where winds are not as well represented are hurricane/tropical storm dominated areas (buoy 42001 in Fig. 7). This is because even with the higher spatial resolution, CFSR is still limited in reproducing these storms (Cox et al., 2011). More examples can be found in the supporting material.

5. Validation using overall significant wave height (Hs)

5.1. Altimeter comparisons

Altimeters provide a direct estimate of H_s, and hence provide a valuable validation tool, especially in the Southern Hemisphere

Please cite this article in press as: Chawla, A., et al. Validation of a thirty year wave hindcast using the Climate Forecast System Reanalysis winds. Ocean Modell. (2012), http://dx.doi.org/10.1016/j.ocemod.2012.07.005

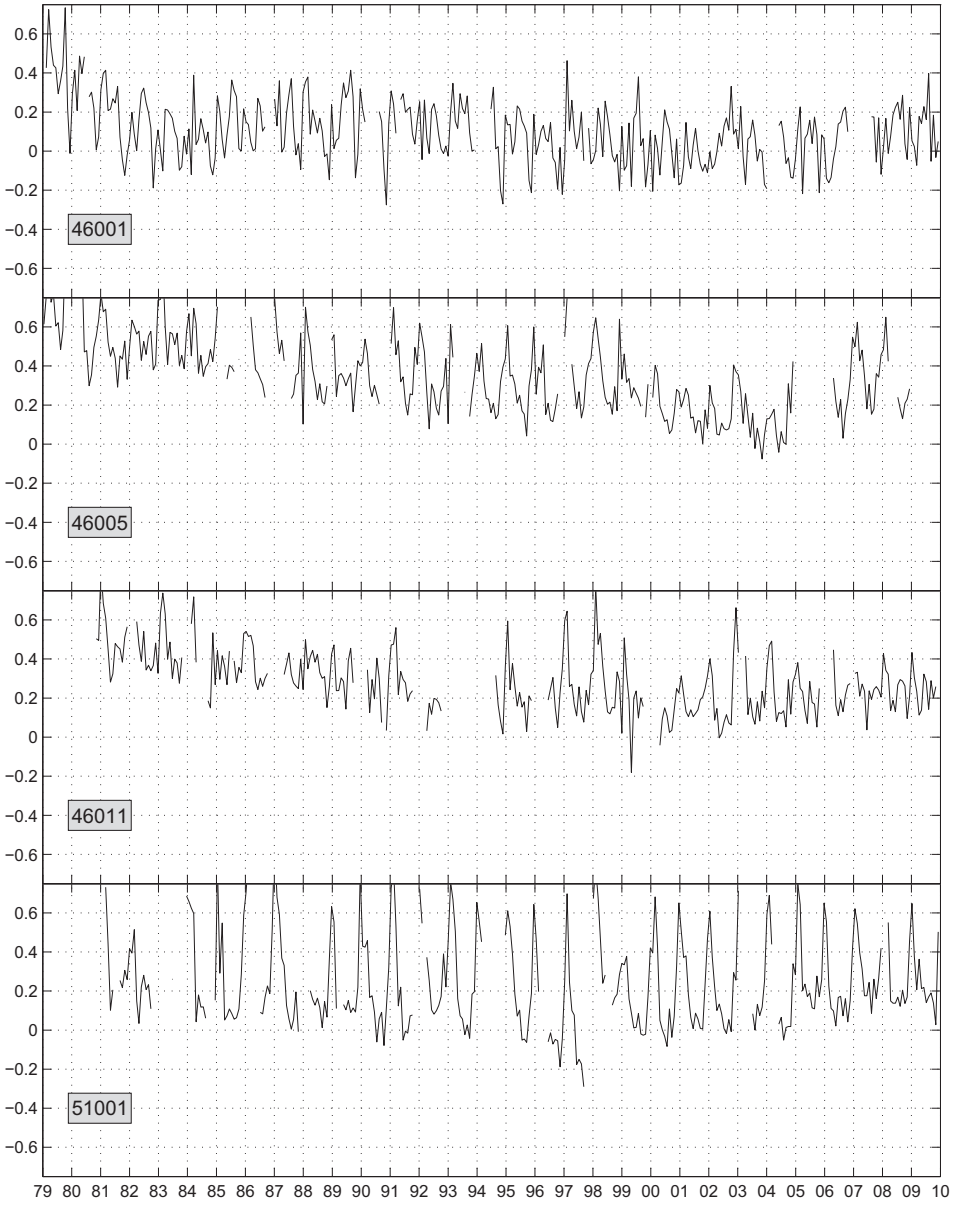

Fig. 15. Like Fig. 14 but for buoys in the Pacific Ocean. H_s units in m.

where limited in situ validation data are available. Error statistics for H_s were computed for the collocated data sets in three month segments to assess the seasonal and interannual variabilities in model performance. Fig. 9 shows the error statistics against all available altimeters for the global domain. The Scatter Indices (SI) are generally lower after 2000, indicating a reduction in the random errors in the model. This is probably related to a better representation of the wind due to additional sources of data for assimilation. The reduction in Scatter Indices are accompanied by a corresponding increase in the goodness of fit parameter (R^2). Biases show some interesting patterns. Apart from the seasonal patterns (highs during the winter months in the Northern and Southern Hemispheres) there are some significant interannual variabilities. Since these variabilities are seen across the different instruments (with some small differences) they likely represent patterns in the wave model behavior. The overall RMS Error shows similar interannual features, because the biases make up a significant portion of the overall error. Also note that R^2 for H_s systematically increases during the altimeter epoch (Fig. 9 lower right panel). This indicates that the quality of the forcing wind slowly increases with time,likely due to a systematic increase in observations. Thus showing that even a detailed reanalysis will produce only a limited homogeneity in time.

Statistics from collocated tracks were also computed regionally. Fig. 10 shows the bias patterns in the Northern and Southern Hemispheres. The seasonal bias patterns are visible in the Northern Hemisphere with the largest biases occurring during the winter months. These are caused primarily by inadequate swell dissipation in the current formulation of WAVEWATCH III (Ardhuin et al., 2010; Chawla et al., 2009) and are most prominent in the Pacific Ocean (where the biggest swells are observed). The Southern Hemisphere shows a similar seasonal variability during the winter months. The interannual variability that was observed in the global domain (Fig. 9), on the other hand, is only seen in the Southern Hemisphere. The higher biases prior to 1994 match well with the over prediction of the higher winds (Fig. 5). There is an increase in bias in the Southern Hemisphere after 2000 that consists of an increasing trend (2000–2006) and a step like jump (after 2006).

Please cite this article in press as: Chawla, A., et al. Validation of a thirty year wave hindcast using the Climate Forecast System Reanalysis winds. Ocean Modell. (2012), http://dx.doi.org/10.1016/j.ocemod.2012.07.005

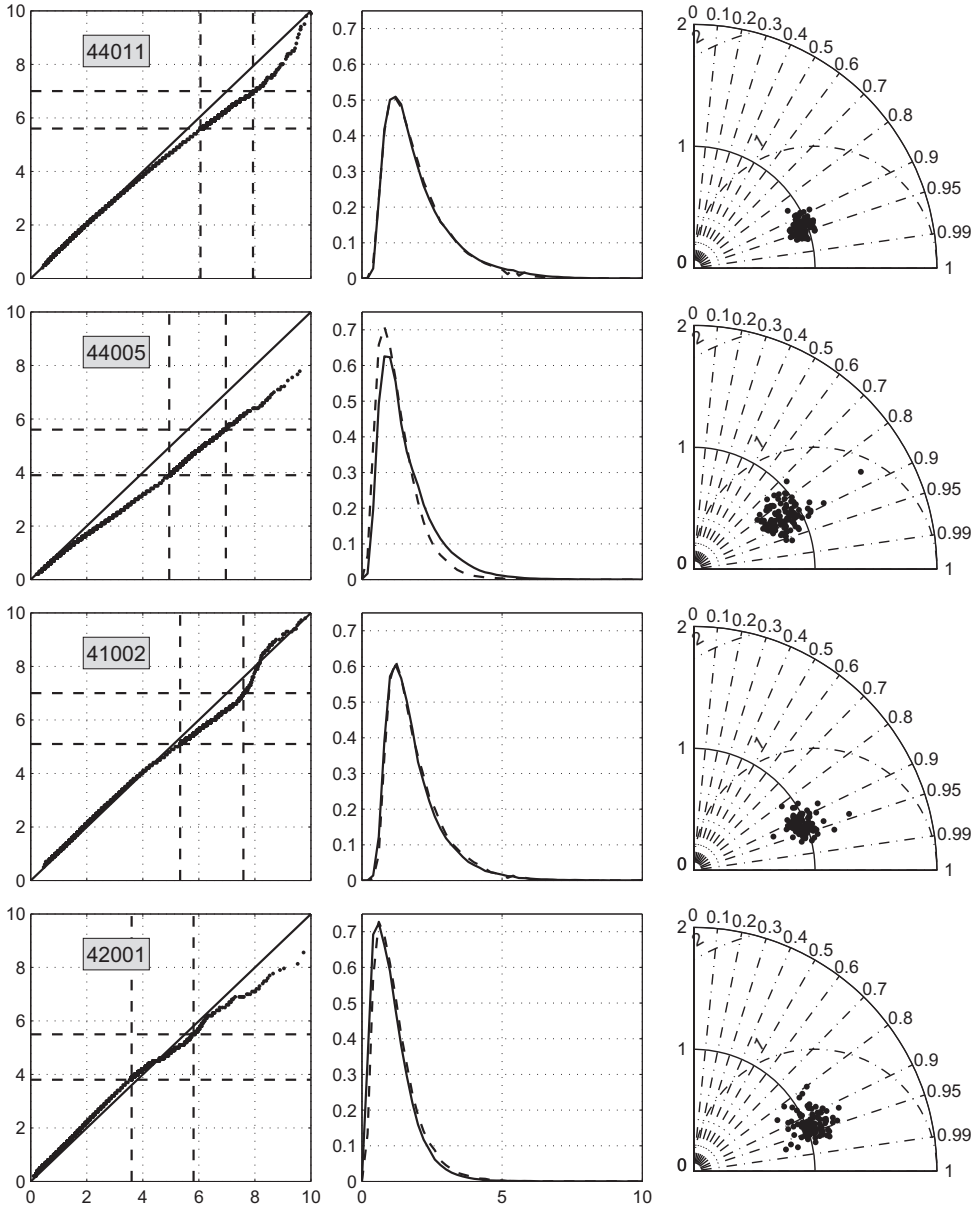

Fig. 16. Like Fig. 7 but for H_s distribution (in m) between model and buoy data.

The jump in the overall bias corresponds with an increase in winds in the CFSR database (Fig. 5). It should be pointed out that the Tolman-Chalikov physics used in this model were last calibrated against global data in 2000–2001 (Tolman et al., 2002) and this coincides (fortuitously) with the lowest overall errors in the domain. Due to the variability in wind speed estimates from the different instruments, it is difficult to determine if the winds were underestimated during this period. Fig. 11 shows the impact of increasing biases in the Southern Hemisphere during December–February between 2002 and 2008. Some of the larger buildups in the biases occur south of 45°S. Apart from the step like increase in biases after 2006, there are also increasing trends in biases between 2000 and 2006 that do not seem to correlate with any changes to wind patterns. Using satellite data, Ardhuin et al. (2011) have shown that icebergs in the Southern Hemisphere play a significant role in blocking the propagation of swells from the lower latitudes to the Western and Southern coastlines in the Southern Hemisphere. In particular they showed a significant increase in iceberg volumes in the Southern Atlantic Ocean in 2004–2005 (see Figs. 3 and 4 in their paper) which matches with the increased biases observed for the same period in the South Atlantic in Fig. 10. They also showed an increasing volume of icebergs in the Pacific Ocean between 2002 and 2006 that could explain the increasing biases in the Southern Pacific.

5.2. Buoy comparisons

Altimeter records only exist back to 1991, and for longer periods of evaluation, validation of H_s has been done using select NDBC buoys, similar to what was done for the CFSR winds. The statistics for the complete records at the buoys can be seen in Table 2. Once again the reader is referred to the supporting material for a more comprehensive set of model-data comparisons.

Figs. 12 and 13 show the time series of H_s at select locations in the Atlantic and Pacific basins respectively. These correspond with the buoys in Figs. 7 and 8. Figs. 14 and 15 show the monthly mean

Please cite this article in press as: Chawla, A., et al. Validation of a thirty year wave hindcast using the Climate Forecast System Reanalysis winds. Ocean Modell. (2012), http://dx.doi.org/10.1016/j.ocemod.2012.07.005

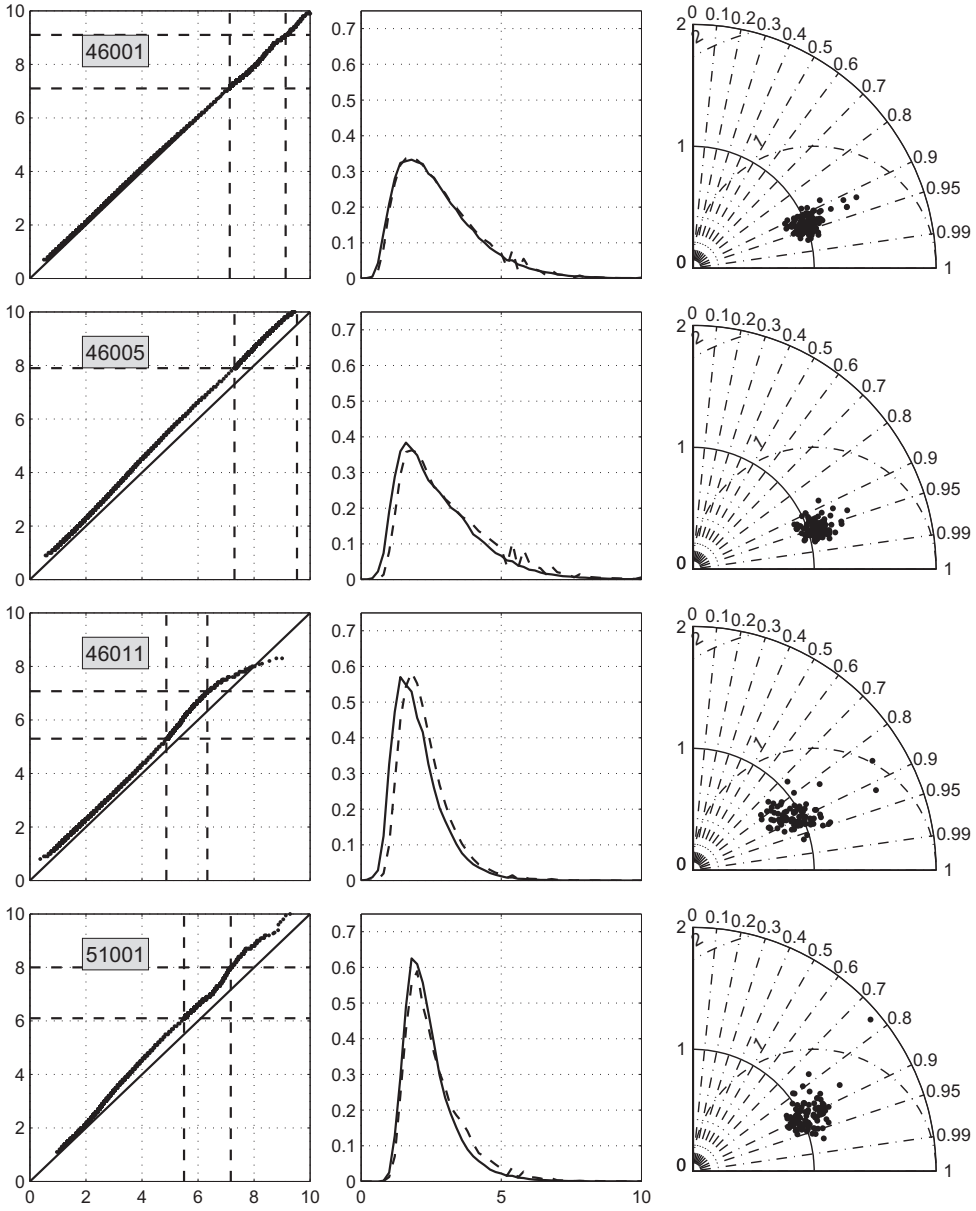

Fig. 17. Like Fig. 16 for buoys in the Pacific Ocean. H_s units in m.

biases in the two basins. Just like in the altimeter data, the biases in the Pacific Ocean are larger than those in the Atlantic. Along the Atlantic coast the biases move from being generally positive at lower latitudes to seasonal patterns with negative biases during the more intensive winter months at the higher latitudes (regions of more active growth). Buoy 44005 is the one buoy that stands out for the poor model – data comparisons, most probably because this buoy is located close to a submarine ridge that is not resolved in the grids. Along the Pacific coast, buoys exposed to swells show a positive bias while those in areas of active growth (buoy 46001) show a mix of positive and negative biases.

The corresponding H_s distributions for the two basins are shown in Figs. 16 and 17. In general the H_s values at the buoys are well represented by the hindcast database, with the PDFs from the model slightly shifted in the Pacific basin due to the over prediction of the swells (Hanson et al., 2009). The Taylor diagrams show a tight cluster around the normalized standard deviation of 1, with a correlation of 0.9 or higher, indicating minimal random errors (buoy 44005 being the one exception).

A peak-over-threshold based analysis was also conducted for the different buoys. Such an analysis focuses more on extreme events, which are important in many applications. Bulk data analysis as presented above do not generally address behavior at extreme events comprehensively. The time series (of H_s) at any particular buoy was separated into different events based on the up-crossing (from below to above) and down-crossing (from above to below) of the time series across a specified threshold. H_s value at the 90th percentile of occurence (computed from observations) has been used as the threshold and is represented by the dashed lines in Figs. 12 and 13. The duration of an event is identified as the time between subsequent up-crossing and down-crossing. Only those events that have a duration greater than 3 h (to identify significant events) and less than 240 h (to exclude cases where buoys stop transmitting data) were chosen. The maximum wave height values

Please cite this article in press as: Chawla, A., et al. Validation of a thirty year wave hindcast using the Climate Forecast System Reanalysis winds. Ocean Modell. (2012), http://dx.doi.org/10.1016/j.ocemod.2012.07.005

Table 3
Peak event analysis. Analysis has been carried out for the same buoys as presented in Table 2. Events are identified when $H_s > H_s^c$, where H_s^c is identified as the 90th percentile of H_s. N is the number of events found for the entire record. All error metrics except SI are in m.

Buoy	N	H_s^c	Bias	SI	RMSE
Atlantic/Gulf of Mexico buoys					
41008	891	1.62	−0.25	15.6	0.40
41004	812	2.27	−0.35	15.4	0.58
41010	825	2.61	−0.20	15.3	0.56
41002	996	3.17	−0.25	15.1	0.69
41001	995	3.60	−0.38	13.2	0.75
44004	1148	3.77	−0.50	13.5	0.84
44025	870	2.23	−0.38	15.6	0.61
44005	1372	2.90	−0.98	18.2	1.21
44011	1053	3.63	−0.56	12.0	0.81
42001	1243	2.03	0.02	17.8	0.50
42002	1316	2.20	−0.07	18.3	0.54
42003	1085	2.01	−0.09	19.0	0.53
42007	951	1.14	−0.43	21.6	0.54
Pacific/Hawaii buoys					
46001	1472	4.67	−0.34	13.2	0.86
46005	1201	4.70	0.18	13.1	0.81
46002	1064	4.51	0.18	12.5	0.74
46006	1070	4.90	0.16	12.5	0.79
46012	1244	3.33	0.17	15.4	0.65
46011	1115	3.20	−0.05	13.8	0.55
51001	1045	3.57	0.17	15.3	0.70
51003	982	3.10	0.18	16.4	0.62
51002	1046	3.23	0.21	15.0	0.58
51004	949	3.20	0.07	12.5	0.46

(in both the model and data) during these events were then compared.

The error statistics together with the number of events for each of the buoys and the corresponding threshold H_s are listed in Table 3 and the scatter plots for select buoys in the two basins are shown in Figs. 18 and 19. In general, the model under predicts the highest waves, with the overall bias being positive in the Pacific Ocean buoys due to the larger number of swell systems in these regions. This appears to be associated with the accurate representation of some but not all extreme events in the CFSR wind fields as described above and as illustrated in Cox et al. (2011). There are also some concerns on the quality of the data for the higher waves (discussed in Section 6).

6. Conclusion and outlook

A global hindcast 31 year archive of evolving wind waves has been developed using the latest reanalysis winds from NCEP and the default model setup of WAVEWATCH III version 3.14. The hindcast archive includes high resolution grids to adequately resolve semi-enclosed basins like the Mediterranean Sea, and areas with an abundance of coastal observations (North America, Northern Europe, Iceland and Australia).

Integral spectral parameters of the archive have been quantitatively validated against both altimeter and buoy data. A supporting manuscript that provides model skill at a large number of NDBC buoys not shown in this paper has also been provided. In the Northern Hemisphere, the statistics show a seasonal pattern. Overall the H_s values are well represented by the model over the entire record of the database with agreement out to 99.9th percentile. In the Southern Hemisphere, there are some concerns that the stronger winds are over predicted in the CFSR prior to 1994, leading to an over prediction in the ocean waves as well. There has also been an increase in the wave heights after 2000 which are probably related to a combined effect of strengthening atmospheric winds and movement of icebergs in this region (Ardhuin et al., 2011). Because the wave model physics were tuned in the intermediate period, positive biases occur in the Southern Hemisphere prior to 1994 and after 2000. While wind intensification and iceberg distribution seem to provide reasonable explanation of wave height biases in the Southern Hemisphere, there may be other possible mechanisms. An event-based analysis indicates that the extreme events are reasonably reproduced in the hindcast. However, the

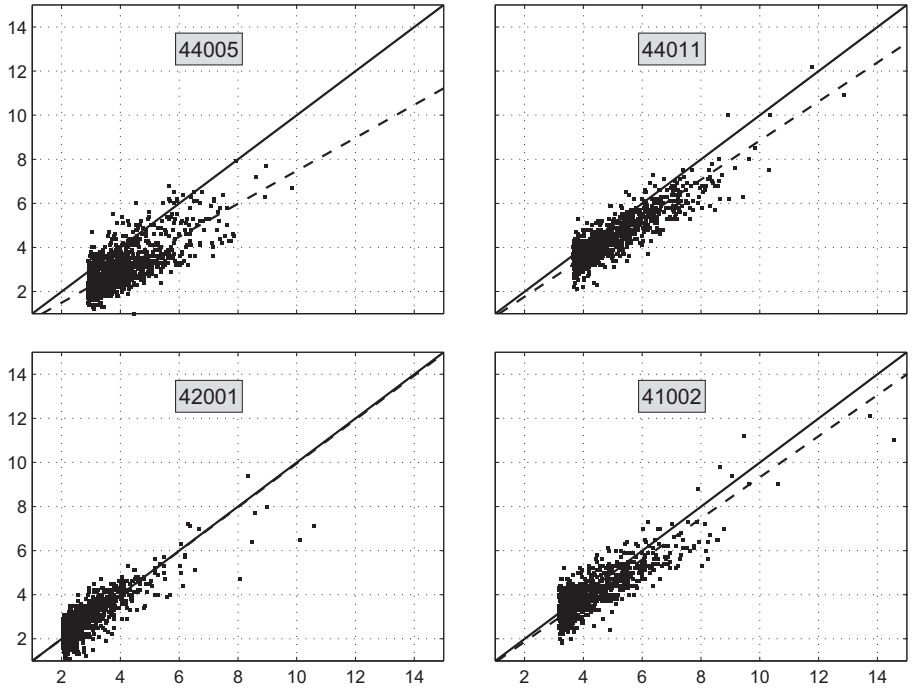

Fig. 18. Scatter plot of peak-over-threshold maximum wave height H_s (in m) for model (y-axis) and data (x-axis) for select buoys in the Atlantic Ocean. See text for how the peak-over-threshold values are defined. Dashed line indicates the linear best fit with zero intercept.

Please cite this article in press as: Chawla, A., et al. Validation of a thirty year wave hindcast using the Climate Forecast System Reanalysis winds. Ocean Modell. (2012), http://dx.doi.org/10.1016/j.ocemod.2012.07.005

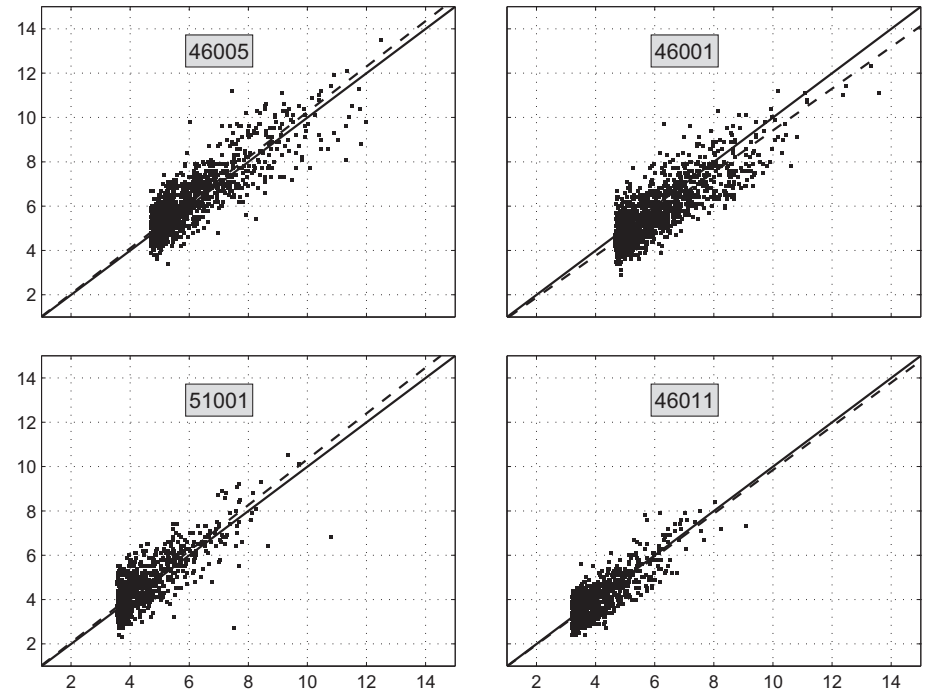

Fig. 19. Like Fig. 18 for buoys in the Pacific Ocean. H_s units in m.

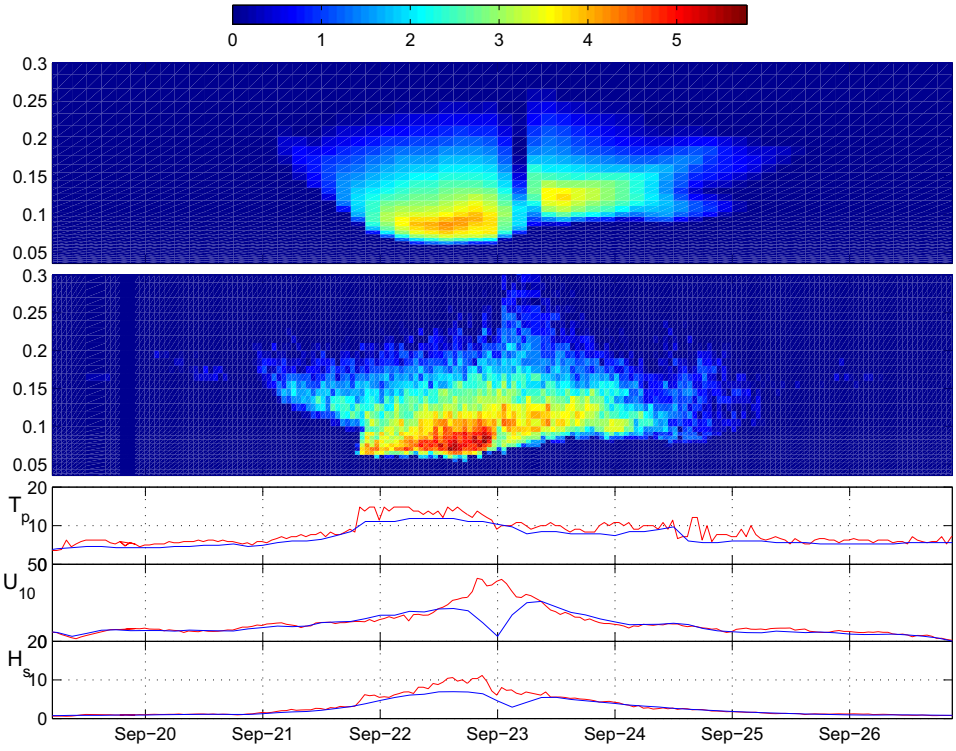

Fig. 20. Spectral comparison at buoy 42001 from September 19th–September 26th 2005. Time series plots of H_s (in m), U_{10} (in m/s) and peak period T_p (in seconds) has the model in blue and data in red. The top two panels show the wave spectra (in m^2/Hz) in a logarithmic scale as a function of frequency (Hz) and time. Top panel is model and second (from the top) panel is observations. (For interpretation of the references to colour in this figure legend, the reader is referred to the web version of this article.)

CFSR wind reproduce some but not all extreme wave events (see Cox et al., 2011), resulting in under representation of the highest waves. Some of which is probably driven by the underlying physics of the wave model.

A final note to address the quality of wave data. Significant wave heights from the buoys have always been used as "Ground Truth" in model validation studies. However, recent work on this by Bender et al. (2010) has shown that buoys that use a 1D

Please cite this article in press as: Chawla, A., et al. Validation of a thirty year wave hindcast using the Climate Forecast System Reanalysis winds. Ocean Modell. (2012), http://dx.doi.org/10.1016/j.ocemod.2012.07.005

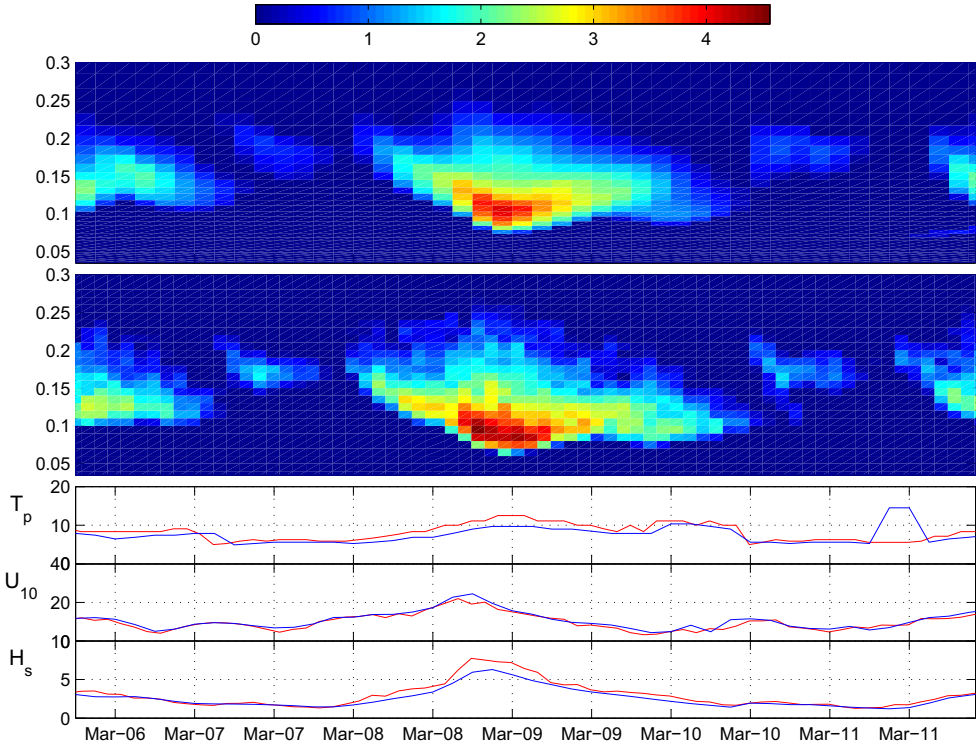

Fig. 21. Like Fig. 20 for buoy 41002 from March 6th–March 11th 2005.

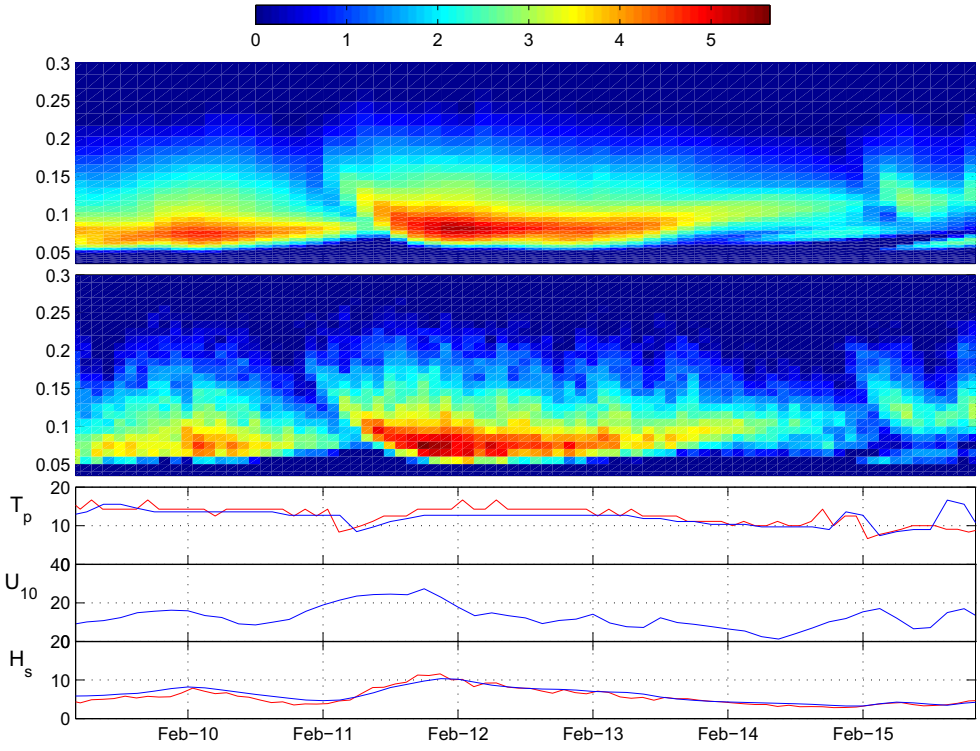

Fig. 22. Like Fig. 20 for buoy 46005 from February 9th–February 15th 1999.

strapped down accelerometer to record waves can have significant errors when the instrument orientation moves away from being vertical. This is a major concern during the larger events since the errors they note in their publication are on the order (and sometimes greater) than the model-data comparisons observed here. A review of historical buoy records is beyond the scope of the present study but needs to be carried out for accurate validations using the algorithms provided in Bender et al. (2010) to correct for errors related to buoy tilt. Apart from this, there are also systematic differences in reported wave measurements from

Please cite this article in press as: Chawla, A., et al. Validation of a thirty year wave hindcast using the Climate Forecast System Reanalysis winds. Ocean Modell. (2012), http://dx.doi.org/10.1016/j.ocemod.2012.07.005

different agencies (Durrant et al., 2009). For the development of wave models as well as undertaking engineering and/or climatic studies a reliable network of "Ground Truth" data is essential. To address this a pilot project has been launched to evaluate wave measurement platforms across the world (Swail et al., 2009).

The next step is to develop a detailed spectral evaluation of the hindcast database. The difficulty with validating wave spectra across a long-term database, is that unlike the integral parameters there are no standard objective statistical measures easily applicable. Some techniques such as using partitioning algorithms to compute integrals over part of the spectrum (Hanson et al., 2009), tracking well separated (in frequency space) swell events (Wingeart et al., 2001), comparing integral parameters across selected frequency ranges of the spectrum (Li and Holt, 2009), or using spectral moments that describe physical processes (Ardhuin et al., 2009) have been developed. To get an indication of how well the wave spectra are reproduced in the hindcasts, qualitative comparisons have been done at select locations for specific events using spectral-time Hovmöller plots (Figs. 20–22). The events have been identified using the peak-over-threshold analysis of the previous section. Since the buoys do not record a true 2D spectrum, comparisons have been limited to the 1D frequency spectra. Buoys (chosen at random) from three different regions – Gulf, Atlantic and Pacific – were selected. At each buoy, one of the larger events (for which spectral data was available) have been shown. Fig. 20 shows the spectra at buoy 42001 in the Gulf of Mexico during hurricane Rita, highlighting the difficulty CFSR has in representing hurricane conditions, with part of the eye of the hurricane passing erroneously over the buoy in the CFSR. A similar feature was observed at this buoy in 2002 during hurricane Lili (figure not shown). In events which do not involve hurricanes (Fig. 21), the spectral comparison is excellent, with the model doing a good job in simulating the growth and down shifting of the spectrum in increasing winds. As a result of the DIA parametrization used in the Tolman-Chalikov physics package the down shifting of the spectral peak is not as intense in the model as in the data, leading to an under prediction in peak period (T_p) around the time when the peak of the storm passes over the buoy. The energy input into the waves during increasing winds is less in the model compared to data. This is a known issue with the Tolman-Chalikov physics (Ardhuin et al., 2007), that was necessary to minimize errors over the entire ocean basin Tolman and September (2002b). The over prediction of swell (Hanson et al., 2009) in the Pacific Ocean can be seen in the wave spectra of Fig. 22 prior to February 11th. Keep in mind that this is just a first step qualitative assessment of the degree of reliability with which ocean conditions (beyond bulk properties) are reproduced in the database. A separate quantitative assessment of the evolution of the wave spectra shall be carried out later.

This database has been developed partially in support of a NOPP initiative to improve operational wave modeling (Tolman et al., submitted for publication). The first stage of developing a 30 year hindcast in the context of the NOPP project, which has been completed and reported here, provides the baseline skill of the default version 3.14 of the WAVEWATCH III model. The second stage, scheduled to be performed in the near future, involves recreating a hindcast database using the (Ardhuin et al., 2010) physics package, which has been added to WAVEWATCH III as part of the NOPP project and was also recently (May 2012) transitioned into operations at NCEP. This package has shown considerable improvement in model skill over the Tolman-Chalikov physics (as documented in Tolman et al. (submitted for publication)). Higher resolution grids will also be introduced for the coastal and regional waters of Canada. If feasible, a curvilinear grid will be introduced for the polar ice caps to extend the computational domain further north. Finally, statistical correction for wind speeds will be considered to remove the discontinuous behavior of high-percentile winds in 1994 and 2006 as illustrated in Fig. 4. The final stage of the database will be developed at the culmination of the NOPP project, and will depend upon the outcome of that project.

The aim of this database is not only to provide long-term archives with multiple physics packages that can then be mined to compare and validate under different physical environments, but also to provide accurate long-term wave records for climatic and/or engineering studies. It should be emphasized that this database has been developed directly from reanalysis winds without any effort to either kinematically correct the winds (Swail and Cox, 2000) or the wave model results (Caires and Sterl, 2005). This does not preclude the need for correction since the database has its own limitations but it does provide a better starting point for these and other correction techniques.

Appendix A. Metrics

To quantify model skill, the standard error metrics of mean bias (b), root mean square error ($RMSE$) and Scatter Index (SI) are used. These are defined as follows

$$b = \overline{y_m - y_o} \tag{A.1}$$

$$RMSE = \sqrt{\overline{(y_m - y_o)^2}} \tag{A.2}$$

$$SI = \frac{\sqrt{\overline{((y_m - \overline{y_m}) - (y_o - \overline{y_o}))^2}}}{\overline{y_o}} * 100 \tag{A.3}$$

where y is the variable, and the subscripts m and o refer to model and observations respectively. The overbar ($\overline{y}$) refers to the average of y over all the samples in the sampling window.

A goodness of fit parameter (R^2) is also used to quantify how well the model fits the data. It is defined as

$$R^2 = \frac{\overline{(y_m - \overline{y_m})^2}}{\overline{(m * y_o + c - \overline{y_m})^2}} \tag{A.4}$$

where m and c are the slope and intercept corresponding to a linear regression fit between model and observations and are given by

$$m = \frac{\overline{y_m y_o} - (\overline{y_m})(\overline{y_o})}{\overline{y_o^2} - (\overline{y_o})^2} \tag{A.5}$$

$$c = \frac{(\overline{y_m}) * \overline{y_o^2} - (\overline{y_o})\overline{y_m y_o}}{\overline{y_o^2} - (\overline{y_o})^2} \tag{A.6}$$

Taylor diagrams (Taylor, 2001) are also used to display multiple metrics together. The error metrics used in the generation of the Taylor diagrams are the correlation coefficient (ρ), the normalized centered root mean square error ($CRMSE$), and the normalized standard deviation (σ_n). These are given by

$$\rho = \frac{\overline{(y_m - \overline{y_m})(y_o - \overline{y_o})}}{\left(\sqrt{\overline{(y_m - \overline{y_m})^2}}\right)\left(\sqrt{\overline{(y_o - \overline{y_o})^2}}\right)} \tag{A.7}$$

$$CRMSE = \frac{\sqrt{\overline{((y_m - \overline{y_m}) - (y_o - \overline{y_o}))^2}}}{\sqrt{\overline{(y_o - \overline{y_o})^2}}} \tag{A.8}$$

$$\sigma_n == \frac{\sqrt{\overline{(y_m - \overline{y_m})^2}}}{\sqrt{\overline{(y_o - \overline{y_o})^2}}} \tag{A.9}$$

Note that $CRMSE$ and σ_n are normalized by observations to facilitate comparisons across different time periods.

Please cite this article in press as: Chawla, A., et al. Validation of a thirty year wave hindcast using the Climate Forecast System Reanalysis winds. Ocean Modell. (2012), http://dx.doi.org/10.1016/j.ocemod.2012.07.005

Appendix B. Supplementary data

Supplementary data associated with this article can be found, in the online version, at http://dx.doi.org/10.1016/j.ocemod.2012.07.005.

References

Amante, C., Eakins, B.W., 2009. Etopo1 1 Arc Minute Global Relief Model: Prodecures, Data Sources and Analysis. NOAA Technical Memorandum NGDC-24, NESDIS, 19 pp.

Ardhuin, F., Herbers, T.H.C., Vledder, G.P.V., Watts, K.P., Jensen, R., Graber, H.C., 2007. Swell and slanting – fetch effects on wind wave growth. J. Phys. Oceanogr. 37, 908–931.

Ardhuin, F., Marie, L., Rascle, N., Forget, P., Roland, A., 2009. Observation and estimation of Lagrangian, Stokes, and Eulerian currents induced by wind and waves at the sea surface. J. Phys. Oceanogr. 39, 2820–2838.

Ardhuin, F., Rogers, E., Babanin, A., Filipot, J.-F., Magne, R., Roland, A., Westhuysen, A.V., Queffeulou, P., Lefevre, J.-M., Aouf, L., Collard, F., 2010. Semi-empirical dissipation source functions for ocean waves: Part 1. Definition, calibration and validation. J. Phys. Oceanogr. 40, 1917–1941.

Ardhuin, F., Tournadre, J., Queffeulou, P., Girard-Ardhuin, F., Collard, F., 2011. Observation and parametrization of small icebergs: drifting breakwaters in the southern ocean. Ocean Modell. 39, 405–410.

Battjes, J.A., Janssen, J.P.F.M., 1978. Energy loss and set-up due to breaking of random waves. In: Proceedings of 16th International Conference on Coastal Engineering. ASCE, pp. 569–587.

Bender, L.C., Guinasso Jr., N.L., Walpert, J.N., Howen, S.D., 2010. A comparison of methods for determining significant wave height – applied to a 3m discus buoy during hurricane Katrina. J. Atmos. Oceanic Technol. 27, 1012–1028.

Caires, S., Sterl, A., 2003. Validation of ocean wind and wave data using triple collocation. J. Geophys. Res. 108 (C3), 43-1–43-15.

Caires, S., Sterl, A., 2005. A new nonparametric method to correct model data: application to significant wave height from the ERA-40 re-analysis. J. Atmos. Oceanic Technol. 22, 443–459.

Caires, S., Sterl, A., Bidlot, J.-R., Graham, N., Swail, V., 2004. Intercomparison of different wind-wave reanalysis. J. Climate 17 (10), 1893–1913.

Chawla, A., Tolman, H.L., 2007. Automated Grid Generation for WAVEWATCH III. Technical Note 254, NCEP/NOAA/NWS, National Center for Environmental Prediction, Washington DC.

Chawla, A., Tolman, H.L., 2008. Obstruction grids for spectral wave models. Ocean Modell. 22, 12–25.

Chawla, A., Tolman, H.L., Hanson, J.L., Devaliere, E.-M., Gerald, V.M., 2009. Validation of a multi-grid wavewatch iii modelling system. In: 11th International Workshop on Wave Hindcasting and Forecasting & Coastal Hazards Symposium. JCOMM Tech. Rep. 52, WMO/TD-No. 1533.

Cox, A.T., Cardone, V.J., Swail, V.R., 2011. On the use of the climate forecast system reanalysis wind forcing in ocean response modeling. In: 12th International Workshop on Wave Hindcasting and Forcasting & 3rd Coastal Hazards Symposium, pp. 20, Paper G3.

Cox, A.T., Swail, V.R., 2001. A global wave hindcast over the period 1958–1997: validation and climate assessment. J. Geophys. Res. 106 (C2), 2313–2329.

Davis, R.W., More, E.F., 1982. A numerical study of vortex shedding from rectangles. J. Fluid Mech. 116, 475–506.

Durrant, T.H., Greenslade, D.J.M., Simmonds, I., 2009. Validation of Jason-1 and Envisat remotely sensed wave heights. J. Atmos. Oceanic Technol. 26, 123–134.

Foristall, G.Z., Heideman, J.C., Leggett, I.M., Roskam, B., Vanderschuren, L., 1996. Effect of sampling variability on hindcast and measured wave heights. J. Waterway Ports Coast. Ocean Eng. 122, 216–225.

Gourrion, J., Vandemark, D., Bailey, S., Chapron, B., Gommenginger, C.P., Challenor, P.G., Srokosc, M.A., 2002. A two parameter wind speed algorithm for Ku-band altimeters. J. Atmos. Oceanic Technol. 19 (12), 2030–2048.

Hanson, J.L., Tracy, B.A., Tolman, H.L., Scott, R.D., 2009. Pacific hindcast performance of three numerical wave models. J. Atmos. Oceanic Technol. 26, 1614–1633.

Hasselmann, K., Barnett, T.P., Bouws, E., Carlson, H., Cartwright, D.E., Enke, K., Ewing, J.A., Gienapp, H., Hasselmann, D.E., Kruseman, P., Meerburg, A., Mueller, P., Olbers, D.J., Richter, K., Sell, W., Walden, H., 1973. Measurements of wind-wave growth and swell decay during the Joint North Sea Wave Project (JONSWAP). Ergaenzungsheft zur Deutschen Hydrographischen Zeitschrift, Reihe A(8) 12, 95 pp.

Hasselmann, S., Hasselmann, K., Allender, J.H., Barnett, T.P., 1985. Computations and parametrizations of the nonlinear energy transfer in a gravity-wave spectrum, Part II: Parametrizations of the nonlinear energy transfer for applications in wave models. J. Phys. Oceanogr. 15, 1378–1391.

Kalnay, E., Kanamitsu, M., Kistler, R., Collins, W., Deaven, D., Gandin, L., Iredell, M., Saha, S., White, G., Woollen, J., Zhu, Y., Leetmaa, A., Reynolds, R., Chelliah, M., Ebisuzaki, W., Higgins, W., Janowiak, J., Mo, K.C., Ropelewski, C., Wang, J., Jenne, R., Joseph, D., 1996. The NCEP/NCAR 40-year reanalysis project. Bull. Am. Meteorol. Soc. 77, 437–471.

Kanamitsu, M., Ebisuzaki, W., Woollen, J., Yang, S.K., Hnilo, J.J., Fiorino, M., Potter, G.L., 2002. NCEP-DOE AMIP-II Reanalysis (R-2). Bull. Am. Meteorol. Soc. 83, 1631–1643.

Leonard, B.P., 1979. A stable and accurate convective modelling procedure based on quadratic upstream interpolation. Comput. Methods Appl. Mech. Eng. 18, 59–98.

Leonard, B.P., 1991. The ULTIMATE conservative difference scheme applied to unsteady one-dimensional advection. Comput. Methods Appl. Mech. Eng. 88, 17–74.

Li, J.-G., Holt, M., 2009. Comparison of envisat asar ocean wave spectra with buoy and altimeter data via a wave model. J. Atmos. Oceanic Technol. 26, 593–614.

Moorthi, S., Pan, H.-L., Caplan, P., 2001. Changes to the 2001 ncep Operational MRF/AVN Global Analysis/Forecast System. Technical Procedures Bulletin 484, NWS/NCEP.

Queffeulou, P., 2004. Long term validation of wave height measurement from altimeters. Mar. Geod. 27, 495–510.

Saha, S., Moorthi, S., Pan, H., Wu, X., Wang, J., Nadiga, S., Tripp, P., Kistler, R., Wollen, J., Behringer, D., Liu, H., Stokes, D., Grumbine, R., Gayno, G., Wang, J., Hou, Y., Chuang, H., Juang, H., Sela, J., Iredell, M., Treadon, R., Kleist, D., VanDelst, P., Keyser, D., Derber, J., Ek, M., Meng, J., Wei, H., Yang, R., Lord, S., van den Dool, H., Kumar, A., Wang, W., Long, C., Chelliah, M., Xue, Y., Huang, B., Schemm, J., Ebisuzaki, W., Lin, R., Xie, P., Chen, M., Zhou, S., Higgins, W., Zou, C., Liu, Q., Chen, Y., Han, Y., Cucurull, L., Reynolds, R., Rutledge, G., Goldberg, M., 2010. The NCEP climate forecast system reanalysis. Bull. Am. Meteorol. Soc. 91, 1015–1057.

Sterl, A., Komen, G.J., Cotton, P.D., 1998. Fifteen years of global wave hindcasts using winds from the European Center for Medium-Range Weather Forecast reanalysis: validating the reanalysis winds and assessing the wave climate. J. Geophys. Res. 103 (C3), 5477–5494.

Stopa, J.E., Cheung, K.F., Tolman, H.L., Chawla, A., submitted for publication. Patterns and cycles in the climate forecast system reanalysis wind and wave data. Ocean Modell.

Swail, V., Jensen, R., Lee, B., Turton, J., Thomas, J., Gulev, S., Yelland, M., Etala, P., Meldrum, D., Birkemeier, W., Burnett, W., Warren, G., 2009. Wave measurements, needs and developments for the next decade. In: Proceedings of OceanObs'09, Venice, p. 10.

Swail, V.R., Cox, A.T., 2000. On the use of NCEP/NCAR reanalysis surface marine wind fields for a long-term North Atlantic wave hindcast. J. Atmos. Oceanic Technol. 17, 532–545.

Taylor, K.E., 2001. Summarizing multiple aspects of model performance in a single diagram. J. Geophys. Res. 106 (D7), 7183–7192.

Tolman, H.L., 2002a. Alleviating the garden sprinkler effect in wind wave models. Ocean Modell. 4, 269–289.

Tolman, H.L., 2002b. Validation of WAVEWATCH III Version 1.15 for a Global Domain. Technical Note 213, NCEP/NOAA/NWS, National Center for Environmental Prediction, Washington DC.

Tolman, H.L., 2007a. The 2007 release of WAVEWATCH III. In: 10th International Workshop on Wave Hindcasting and Forecasting & Coastal Hazards Symposium. Paper Q4.

Tolman, H.L., 2007b. Development of a Multi-grid Version of WAVEWATCH III. Tech. Note 256, NOAA/NWS/NCEP/MMAB, 88 pp. + Appendices.

Tolman, H.L., 2008. A mosaic approach to wind wave modeling. Ocean Modell. 25, 35–47.

Tolman, H.L., 2009. User Manual and System Documentation of WAVEWATCH III Version 3.14. Tech. Note 276, NOAA/NWS/NCEP/MMAB, 220 pp.

Tolman, H.L., Balasubramaniyan, B., Burroughs, L.D., Chalikov, D.V., Chao, Y.Y., Chen, H.S., Gerald, V.M., 2002. Development and implementation of wind generated ocean surface wave models at NCEP. Weather Forecast. 17, 311–333.

Tolman, H.L., Banner, M.L., Kaihatu, J.M., submitted for publication. The NOPP operational wave model improvement project. Ocean Modell.

Tolman, H.L., Chalikov, D., 1996. Source terms in a third generation wind wave model. J. Phys. Oceanogr. 26, 2497–2518.

Uppala, S.M., Kallberg, P.W., Simmons, A.J., Andrae, U., Bechtold, V.D.C., Fiorino, M., Gibson, J.K., Haseler, J., Hernandez, A., Kelly, G.A., Li, X., Onogi, K., Saarinen, S., Sokka, N., Allan, R.P., Andersson, E., Arpe, K., Balmaseda, M.A., Beljaars, A.C.M., Berg, L.V.D., Bidlot, J., Bormann, N., Caires, S., Chevallier, F., Dethof, A., Dragosavac, M., Fisher, M., Fuentes, M., Hagemann, S., Hólm, E., Hoskins, B.J., Isaksen, L., Janssen, P.A.E.M., Jenne, R., Mcnally, A.P., Mahfouf, J.-F., Morcrette, J.-J., Rayner, N.A., Saunders, R.W., Simon, P., Sterl, A., Trenberth, K.E., Untch, A., Vasiljevic, D., Viterbo, P., Woollen, J., 2005. The ERA-40 reanalysis. Quart. J. Roy. Meteorol. Soc. 131, 2961–3012.

Wingeart, K.M., O'Reilly, W.C., Herbers, T.H.C., Wittmann, P.A., Jenssen, R.E., Tolman, H.L., 2001. Validation of operational global wave prediction models with spectral buoy data. In: Edge, B.L., Hemsley, J.M. (Eds.), Ocean Wave Measurement and Analysis. ASCE, pp. 590–599.